G331.512-0.103: a template case for astrochemical studies with LLAMA

Nicolás Duronea (Instituto de Astrofísica de La Plata, I.A.L.P.)

L. Bronfman (U. de Chile) E. Mendoza (U. de Sao Pāolo) C. Canelo (U. de Sao Pāolo)

J. Santos (U. de Sao Pāolo) M. Merello (U. de Chile) R. Finger (U. de Chile)

J. Lépine (U. de Sao Pāolo) N Reyes (U. de Chile) C. Cappa (FCAGLP)

M. Arnal (FCAGLP) L. Åke-Nyman (J.A.O.) M. Carvajal (U. de Granada)

A. Friaça (U. de Sao Pāolo) I. Kleiner (U. de Paris-Est) A. Faure (U. de Grenoble-Alpes)

C. Hervias-Caimapo (Florida State Univ.)

Science with LLAMA. September 5-9 2022. Salta, Argentina

Hot Molecular Cores

Massive dense clouds (IRDCs)

↓

Hot Molecular Core

↓

Ultra Compact HII region

↓

Classical HII Region (O- and -B stars)

Hot Molecular Cores

$D < 0.1$ pc

$M \sim 10^3$ Mo

$nH_2 \sim 10^6 - 10^8$ cm^{-3}

$T \sim 100 - 300$ K

$L > 10^4$ Lo

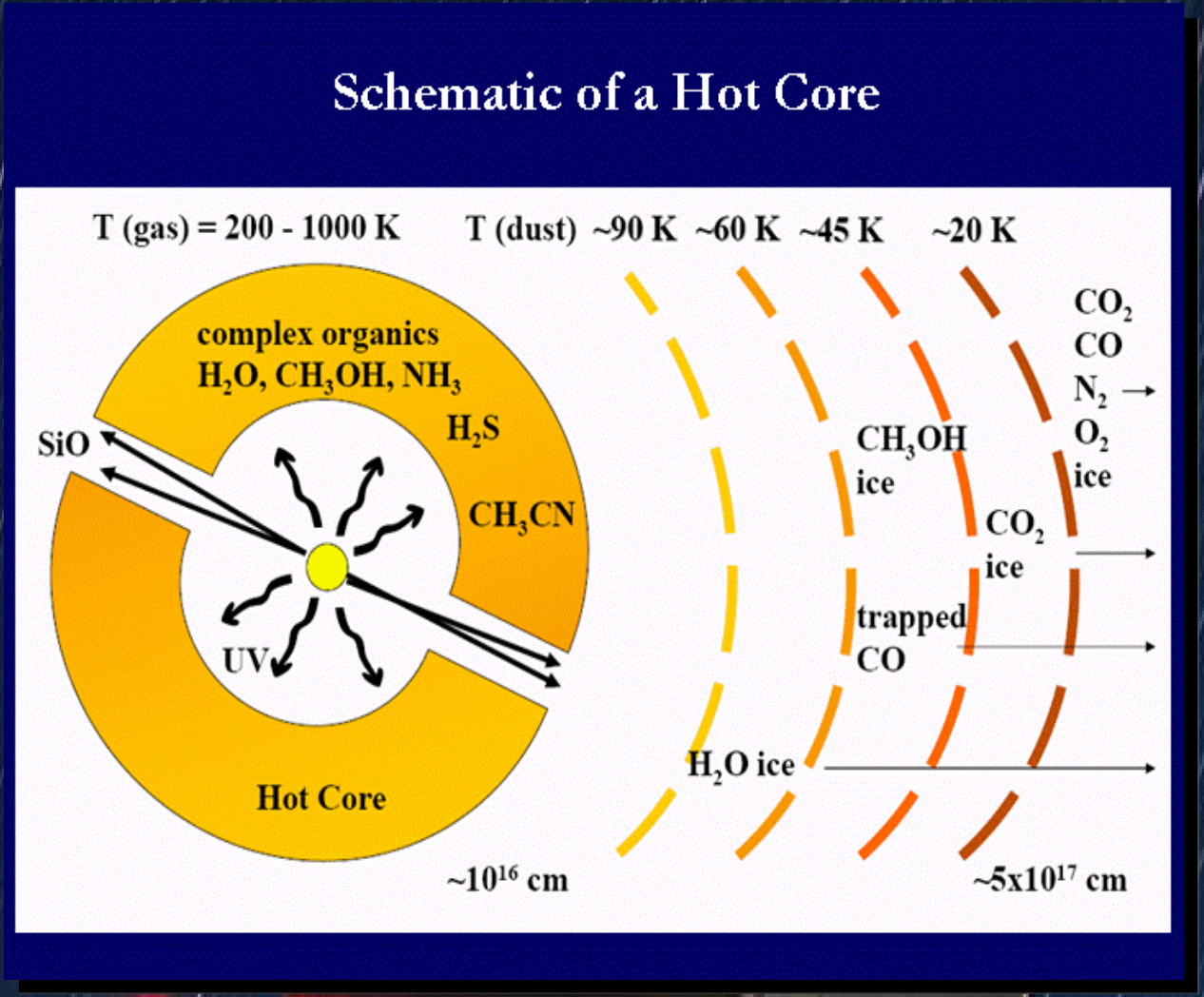

G331.5-0.1

Merello et al. (2013a)

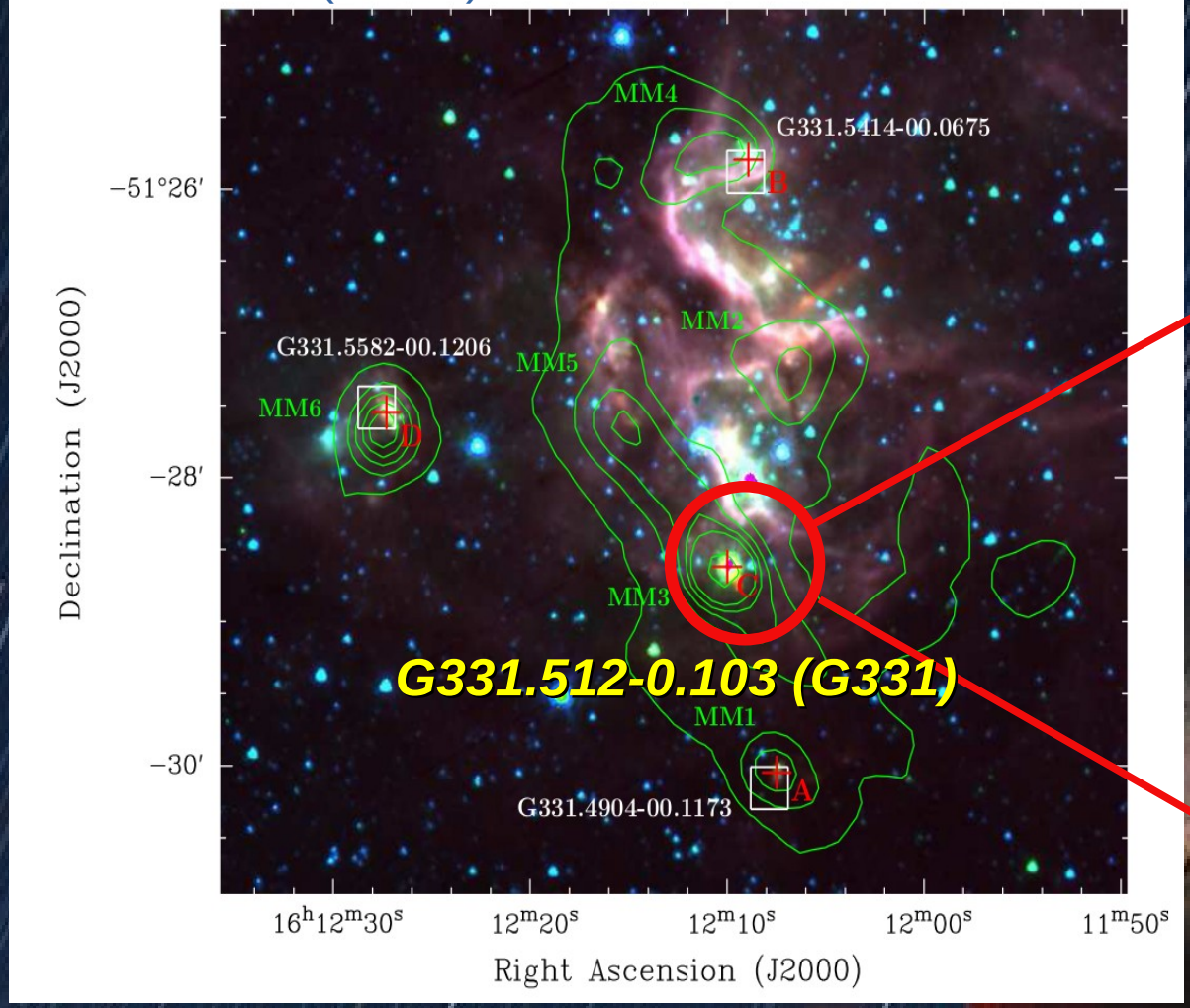

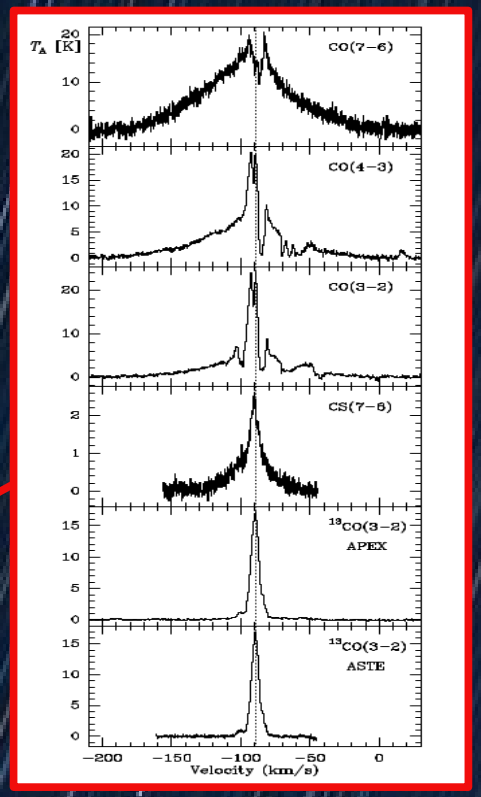

Bronfman et al. (2008)

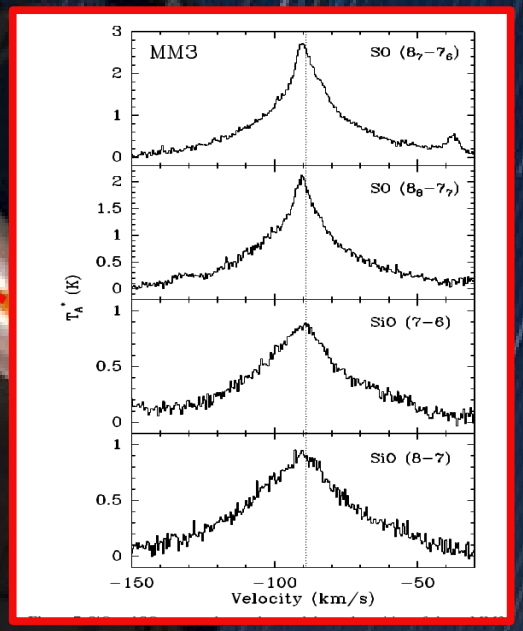

Merello et al. (2013a)

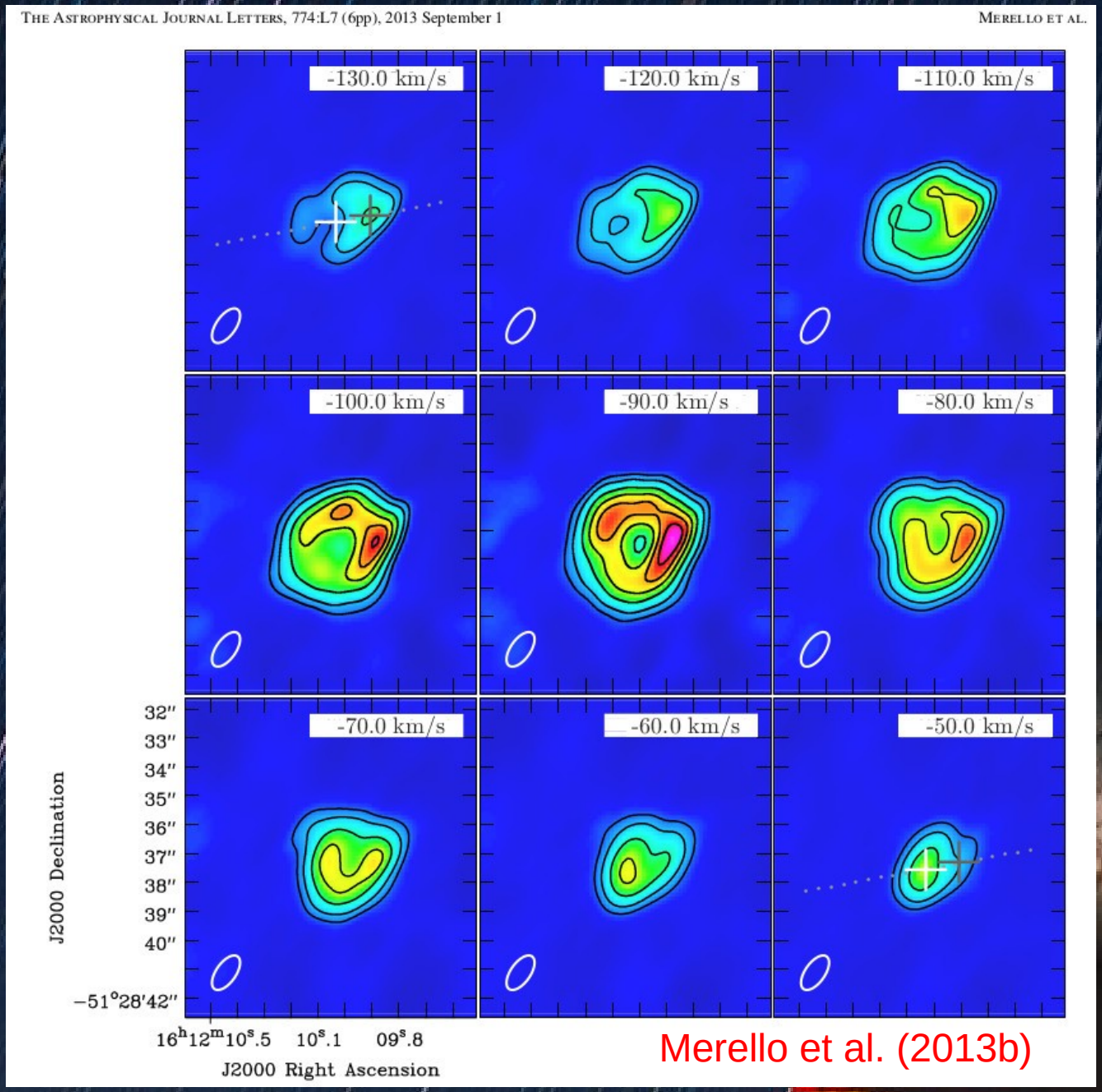

Merello et al. (2013b)

APEX

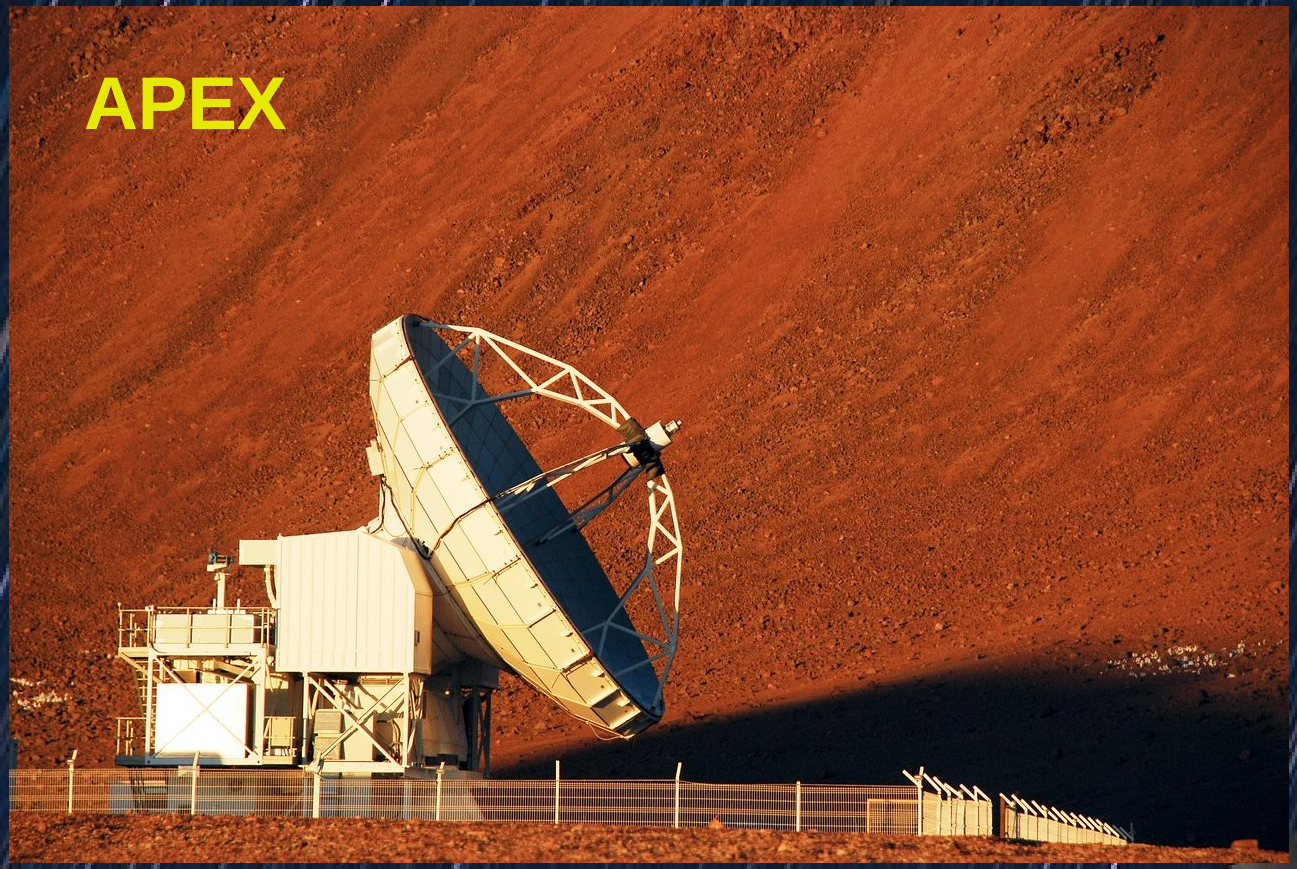

Instrument	Type	Mode	Frequency [GHz]	HPBW [arcsec]	IF range [GHz]	# of beams	Location
APEX-1 *(SHeFI)*	Heterodyne SIS	SSB	213 - 275	30 - 23	4 - 8	1	Nasmyth-A
APEX-2 *(SHeFI)*	Heterodyne SIS	SSB	267 - 378	23 - 17	4 - 8	1	Nasmyth-A
APEX-3 *(SHeFI)*	Heterodyne SIS	DSB	385 - 506	17 - 13	4 - 8	1	Nasmyth-A
APEX-T2 *(SHeFI)*	Heterodyne HEB	DSB	1250 - 1390	5	2 - 4	1	Nasmyth-A

APEX-2

RMS ~ 0.025 K (Ta)

DV = 0.25 km/s

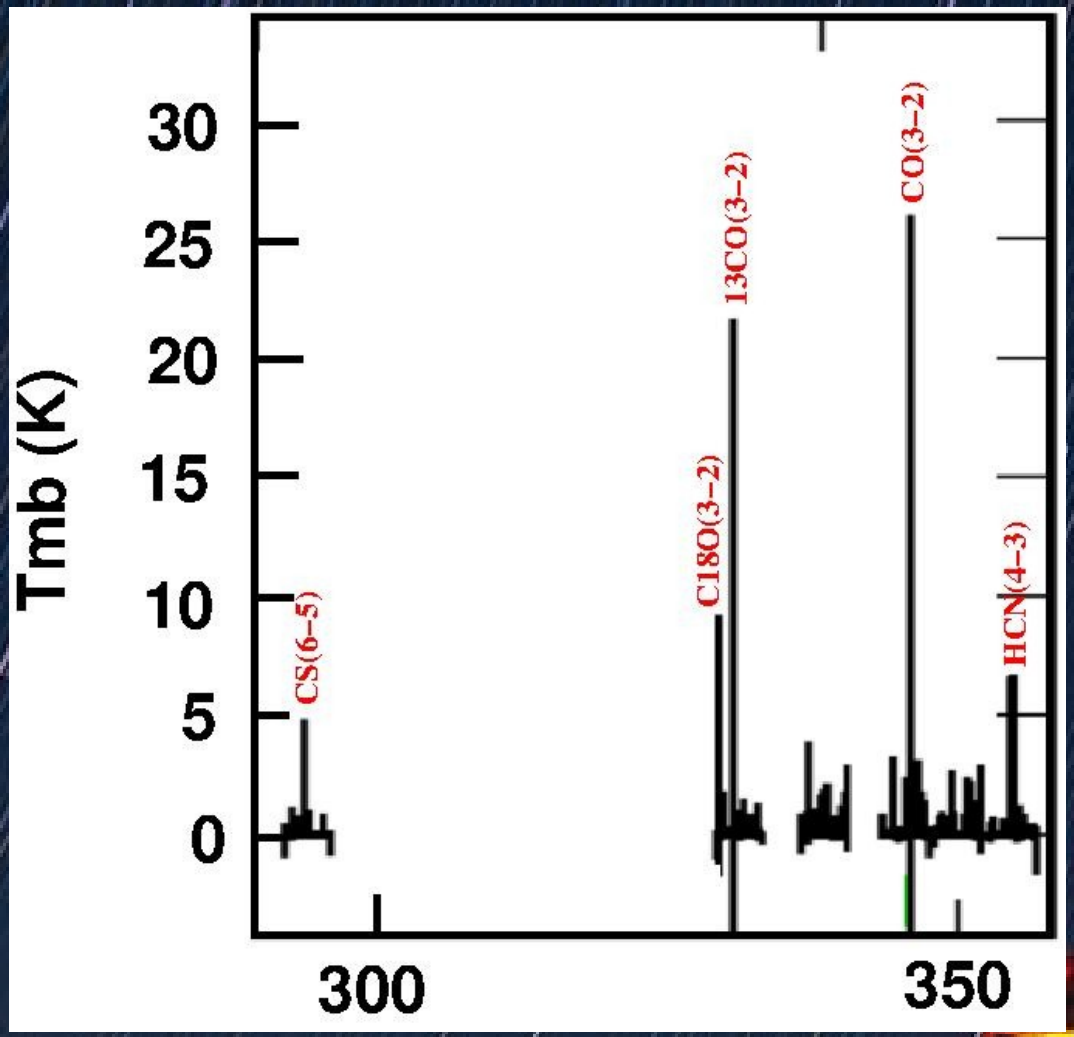

CH_3CN

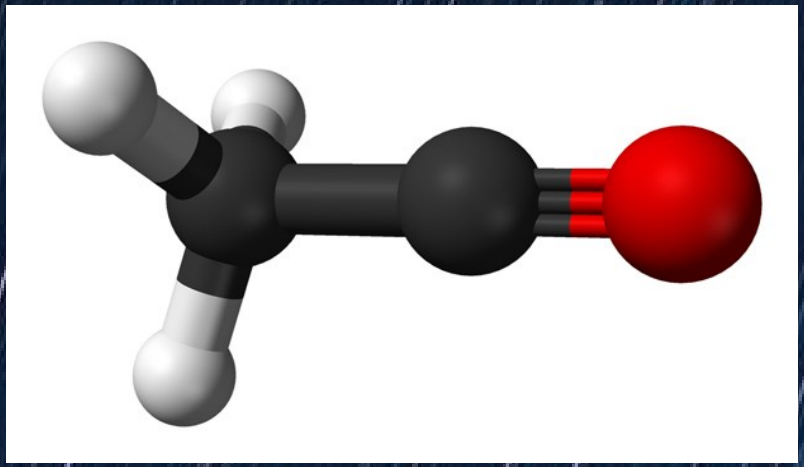

CH_3OH

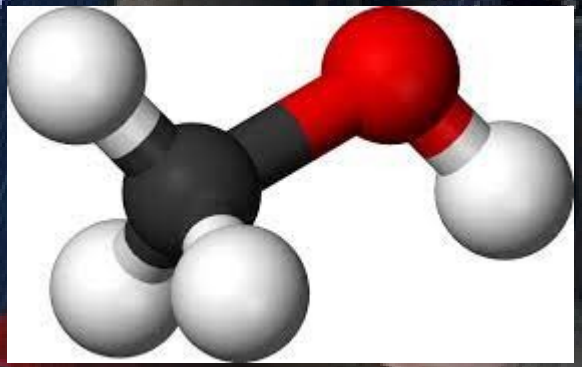

The Astrophysical Journal, 853:152 (12pp), 2018 February 1 https://doi.org/10.3847/1538-4357/aaa1ec
© 2018. The American Astronomical Society. All rights reserved.

G331.512–0.103: An Interstellar Laboratory for Molecular Synthesis. I. The Ortho-to-para Ratios for CH_3OH and CH_3CN

Edgar Mendoza[1], Leonardo Bronfman[2], Nicolas U. Duronea[3], Jacques R. D. Lépine[1], Ricardo Finger[2], Manuel Merello[4], Carlos Hervías-Caimapo[2,5], Diana R. G. Gama[1], Nicolas Reyes[6], and Lars Åke-Nyman[7]
[1] Universidade de São Paulo, IAG Rua do Matão, 1226, Cidade Universitária, 05508-090, São Paulo, Brazil; emendoza@usp.br
[2] Departamento de Astronomía, Universidad de Chile, Casilla 36-D, Santiago de Chile, Chile
[3] Instituto Argentino de Radioastronomía, IAR CONICET, CCT-La Plata, C.C.5., 1894, Villa Elisa, Argentina
[4] Istituto di Astrofisica e Planetologia Spaziali-INAF Via Fosso del Cavaliere 100, I-00133 Roma, Italy
[5] Jodrell Bank Centre for Astrophysics, School of Physics and Astronomy, University of Manchester, Oxford Road, Manchester M139PL, UK
[6] Electrical Engineering Department, Universidad de Chile, Av. Tupper 2007, Santiago, Chile
[7] Joint ALMA Observatory, JAO Alonso de Córdova 31070, Vitacura, Santiago de Chile, Chile
Received 2017 October 14; revised 2017 December 7; accepted 2017 December 12; published 2018 February 1

Abstract

Spectral line surveys reveal rich molecular reservoirs in G331.512–0.103, a compact radio source in the center of an energetic molecular outflow. In this first work, we analyze the physical conditions of the source by means of CH_3OH and CH_3CN. The observations were performed with the APEX Telescope. Six different system configurations were defined to cover most of the band within (292–356) GHz; as a consequence, we detected a forest of lines toward the central core. A total of 70 lines of A/E–CH_3OH and A/E–CH_3CN were analyzed, including torsionally excited transitions of CH_3OH ($\nu_t = 1$). In a search for all the isotopologues, we identified transitions of $^{13}CH_3OH$. The physical conditions were derived considering collisional and radiative processes. We found common temperatures for each A and E symmetry of CH_3OH and CH_3CN; the derived column densities indicate an A/E equilibrated ratio for both tracers. The results reveal that CH_3CN and CH_3OH trace a hot and cold component with $T_k \sim 141$ K and $T_k \sim 74$ K, respectively. In agreement with previous ALMA observations, the models show that the emission region is compact ($\lesssim 5''.5$) with gas density $n(H_2) = (0.7\text{–}1)\times 10^7$ cm^{-3}. The CH_3OH/CH_3CN abundance ratio and the evidences for prebiotic and complex organic molecules suggest a rich and active chemistry toward G331.512–0.103.

Key words: ISM: molecules – molecular processes – radio lines: ISM

1. Introduction

G331.512–0.103 is one of the most luminous and energetic molecular outflows known in the Galaxy. All of the system is embedded in a star-forming region known as G331.5-0.1, located in the Norma spiral arm at a distance of ~7 pc. This source exhibits typical H II region properties and intense maser emission of OH and CH_3OH (Caswell 1998; Nyman et al. 2001; Bronfman et al. 2008). At the center of the system, a young and massive stellar object drives a bipolar flow of around 55 $M_\odot$ with a momentum of $\sim 2.4 \times 10^3$ $M_\odot$ km s^{-1}. Radio continuum observations have revealed a compact and central structure associated with a dust core. The central region has been also mapped with ALMA observations with transitions of SiO (8–7), $H^{13}CO^+$ (4–3), HCO^+ (4–3) and CO (3–2). The observations revealed a ring-like structure, consistent with a cavity, and the existence of a high-velocity outflow emission confined in a region lower than 5″ in size (Merello et al. 2013a, 2013b; Hervías et al. 2015). In this work, we present new results on the emission of CH_3OH and CH_3CN detected toward the central core, denominated hereafter as G331.

As an interstellar laboratory, G331 exhibits active chemistry in prebiotic and complex organic molecules likely stimulated by physical processes in the molecular core and outflow. With the Atacama Pathfinder EXperiment APEX Telescope, we detected a vast number of molecular lines potentially linked to reservoirs traced by CH_3OH and CH_3CN. Those tracers are excellent candidates to unveil the different physical components that O- and N-bearing molecules can reveal toward hot molecular cores (Sandell et al. 1994; Wyrowski et al. 1999; Jørgensen et al. 2004; Beuther et al. 2005; Fontani et al. 2007; Fuente et al. 2014; Giannetti et al. 2017). In addition, from a chemical point of view, CH_3OH and CH_3CN are considered as parent and daughter molecules, respectively, in the route of interstellar molecular formation (e.g., Nomura & Millar 2004). With that motivation, we started a systematic study of G331 beginning with spectral analyses of A/E–CH_3OH and A/E–CH_3CN.

1.1. The Tracers CH_3CN and CH_3OH

CH_3CN (methyl cyanide) is a symmetric top molecule. The nuclear spin state of the hydrogen atoms defines whether the molecule has an ortho (E) or para (A) symmetry. Rotational levels of CH_3CN are characterized by two quantum numbers: the total angular momentum (J) and its projection on the axis of symmetry (K). Spectral signatures are associated to K-ladder structures whose notation for the A and E configurations are $K = 3n$ and $K = 3n \pm 1$, respectively (Solomon et al. 1971; Boucher et al. 1980; Cummins et al. 1983).

CH_3OH (methanol) is one of the simplest asymmetric-top molecules; however, its spectrum is quite complicated because there is a strong coupling between torsional and vibrational modes. Methanol also exists in two species denoted as A and E depending on the nuclear spin alignment of the three H-atoms of the methyl group (CH_3). The energy levels of methanol can be assigned with the total angular momentum J and its component K along the symmetry axis (Lees & Baker 1968; Lovas et al. 1982).

Science with LLAMA. September 5-9 2022. Salta, Argentina

Table 2
Spectral Line Analysis of A–CH_3CN and E–CH_3CN in G331

Transition	Frequency (MHz)	E_u (K)	A_{ij} (10^{-3} s^{-1})	$\int T_{mb} dV$ (K km s^{-1})	V_{lsr} (km s^{-1})	FWHM (km s^{-1})
A–CH_3CN						
[a]16_9–15_9	293845.164	697.83	1.51	…	…	…
16_6–15_6	294098.867	377.0721	1.9	2.065 ± 0.006	−90.7 ± 0.2	10.3 ± 0.5
16_3–15_3	294251.461	184.3532	2.13	5.9 ± 0.3	−90.4 ± 0.2	8.2 ± 0.6
16_0–15_0	294302.388	120.0696	2.21	7.9 ± 0.2	−89.69 ± 0.07	8.8 ± 0.2
[b]$18_9 - 17_9$	330557.569	728.67	2.36	0.15 ± 0.04	−91.2 ± 0.1	0.9 ± 0.2
[c]$18_6 - 17_6$	330842.762	407.9468	2.8	1.53 ± 0.07	−88.2 ± 0.4	10 ± 0.1
$18_3 - 17_3$	331014.296	215.2437	3.07	6.6 ± 0.5	−90.3 ± 0.3	8.9 ± 0.8
$18_0 - 17_0$	331071.544	150.9654	3.16	9.1 ± 0.3	−89.5 ± 0.1	9.4 ± 0.3
[a]$19_9 - 18_9$	348911.401	745.42	2.87	…	…	…
$19_6 - 18_6$	349212.311	424.7065	3.34	3.01 ± 0.01	−90.4 ± 0.2	11.5 ± 0.5
[d]$19_3 - 18_3$	349393.297	232.012	3.63	3.66 ± 0.07	−91.7 ± 0.3	3.8 ± 0.6
$19_0 - 18_0$	349453.7	167.7368	3.72	5.5 ± 0.3	−90.5 ± 0.1	6.8 ± 0.4
E–CH_3CN						
[e]16_8–15_8	293940.916	568.69	1.65	…	…	…
16_7–15_7	294025.496	461.7635	1.78	0.8 ± 0.1	−88.7 ± 0.6	10 ± 2
16_5–15_5	294161.001	290.5519	1.99	2.14 ± 0.09	−89.2 ± 0.2	9.8 ± 0.5
16_4–15_4	294211.873	226.3073	2.07	2.93 ± 0.08	−90.2 ± 0.1	9.3 ± 0.3
16_2–15_2	294279.75	140.6138	2.17	4.19 ± 0.09	−90.79 ± 0.08	7.9 ± 0.2
16_1–15_1	294296.728	119.1843	2.2	7.74 ± 0.07	−91.87 ± 0.07	9.4 ± 0.1
[f]$18_8 - 17_8$	330665.206	599.54	2.52	1.21 ± 0.07	−91.4 ± 0.2	8.1 ± 0.5
$18_7 - 17_7$	330760.284	492.6304	2.67	0.8 ± 0.1	−90.8 ± 0.7	11 ± 2
$18_5 - 17_5$	330912.608	321.4329	2.91	2.9 ± 0.1	−89.4 ± 0.2	11.6 ± 0.6
$18_4 - 17_4$	330969.794	257.1937	3	3.3 ± 0.1	−90.5 ± 0.1	9.2 ± 0.4
$18_2 - 17_2$	331046.096	171.5073	3.12	6.66 ± 0.09	−90.87 ± 0.07	10.4 ± 0.2
$18_1 - 17_1$	331065.181	150.0797	3.15	10.252 ± 0.007	−91.62 ± 0.06	10.6 ± 0.1
[a]$19_8 - 18_8$	349024.971	616.29	3.05	…	…	…
[g]$19_7 - 18_7$	349125.287	509.38	3.2	0.304 ± 0.003	−90.1 ± 0.6	5.9 ± 0.7
$19_5 - 18_5$	349286.006	338.1962	3.45	2.106 ± 0.008	−89.6 ± 0.2	9.5 ± 0.5
[h]$19_4 - 18_4$	349346.343	273.9599	3.55	2.091 ± 0.002	−89.76 ± 0.09	6.1 ± 0.1
$19_2 - 18_2$	349426.85	188.2773	3.67	5.3 ± 0.1	−90.61 ± 0.9	9.8 ± 0.2
$19_1 - 18_1$	349446.987	166.8506	3.71	8.018 ± 0.001	−91.76 ± 0.05	9.39 ± 0.08

Table 3
The Table 2 Caption Applies Here for A–CH_3OH and E–CH_3OH

Transition J_k	Frequency (MHz)	E_u (K)	A_{ij} (10^{-5} s^{-1})	$\int T_{mb} dV$ (K km s^{-1})	V_{lsr} (km s^{-1})	FWHM (km s^{-1})
A–CH_3OH						
6_1–5_1	292672.889	63.707	10.6	6.95 ± 0.06	−90.67 ± 0.02	5.24 ± 0.05
3_2–4_1	293464.055	51.6381	2.89	3.39 ± 0.09	−90.35 ± 0.09	6.8 ± 0.2
12_2–11_3	329632.881	218.8033	6	0.59 ± 0.07	−89.8 ± 0.3	4.1 ± 0.6
11_1–11_0	331502.319	169.0101	19.6	3.394 ± 0.001	−90.17 ± 0.02	2.82 ± 0.03
[a]7_3–8_1	332920.822	114.794	1.15×10^{-5}	…	…	…
12_1–12_0	336865.149	197.0765	20.3	6.9 ± 0.5	−91.9 ± 0.2	6.9 ± 0.3
7_0–6_0	338408.698	64.9817	17	10.83 ± 0.07	−90.51 ± 0.02	5.31 ± 0.04
7_6–6_6	338442.367	258.6994	4.53	1.09 ± 0.06	−91.3 ± 0.1	5.7 ± 0.4
7_5–6_5	338486.322	202.8864	8.38	2.11 ± 0.08	−90.98 ± 0.09	4.9 ± 0.2
7_2–6_2	338512.853	102.7032	15.7	7.3 ± 0.4	−90.5 ± 0.1	5.5 ± 0.4
7_3–6_3	338543.152	114.7948	13.9	9.21 ± 0.08	−89.77 ± 0.02	5.62 ± 0.05
7_2–6_2	338639.802	102.7179	15.7	7.4 ± 0.7	−90.6 ± 0.2	5.6 ± 0.6
2_2–3_1	340141.143	44.6729	2.79	2.14 ± 0.06	−90.71 ± 0.08	5.5 ± 0.2
[a]16_1–15_2	345903.916	332.6545	9.02	…	…	…
5_4–6_3	346204.271	115.1625	2.17	2.31 ± 0.07	−90.74 ± 0.09	5.9 ± 0.2
$14_1 - 14_0$	349106.997	260.2068	22	4.25 ± 0.06	−90.77 ± 0.04	5.41 ± 0.09
1_1–0_0	350905.1	16.841	33.1	12.19 ± 0.05	−90.58 ± 0.01	5.13 ± 0.03
[a]8_2–9_0	351685.48	121.2915	16.2	…	…	…
[a]10_4–11_2	355279.539	207.9929	1.22×10^{-3}	…	…	…
13_0–12_1	355602.945	211.0285	12.6	4.02 ± 0.04	−91.01 ± 0.02	4.76 ± 0.06
15_1–15_0	356007.235	295.2675	23	2.68 ± 0.05	−90.46 ± 0.05	5.8 ± 0.1
E–CH_3OH						
8_{-3}–9_{-2}	330793.887	138.3774	5.38	1.96 ± 0.06	−91.03 ± 0.07	4.6 ± 0.1
16_{-1}–15_{-2}	331220.371	312.7333	5.23	0.55 ± 0.06	−91.4 ± 0.3	5.3 ± 0.6
3_3–4_2	337135.853	53.7412	1.58	1.09 ± 0.06	−91.1 ± 0.1	4.7 ± 0.3
[a]7_2–6_2	337671.238	456.8285	15.5	…	…	…
[a]7_5–6_5	337685.248	486.0568	8.28	…	…	…
[a]7_{-1}–6_{-1}	337707.568	470.3161	16.5	…	…	…
7_0–6_0	338124.488	70.1794	16.9	9.09 ± 0.06	−90.74 ± 0.01	5.01 ± 0.04
7_{-1}–6_{-1}	338344.588	62.6521	16.6	9.61 ± 0.08	−90.63 ± 0.02	4.87 ± 0.05
[a]7_6–6_6	338404.61	235.8941	4.51	…	…	…
[a]7_{-6}–6_{-6}	338430.975	246.0504	4.54	…	…	…
7_{-5}–6_{-5}	338456.536	181.1017	8.34	1.3 ± 0.4	−90.9 ± 0.7	5 ± 2
7_5–6_5	338475.226	193.1625	8.34	1.5 ± 0.6	−91 ± 0.1	5 ± 3
7_{-4}–6_{-4}	338504.065	144.9961	11.5	4 ± 2	−91.3 ± 0.04	6 ± 1
7_4–6_4	338530.257	153.0934	11.5	3.1 ± 0.6	−91.1 ± 0.4	5 ± 1
7_{-3}–6_{-3}	338559.963	119.8084	14	4.5 ± 0.1	−90.93 ± 0.6	5.2 ± 0.1
7_3–6_3	338583.216	104.8115	13.9	6.9 ± 0.2	−90.99 ± 0.08	6.6 ± 0.2
7_1–6_1	338614.936	78.1537	17.1	21.4 ± 0.8	−89.5 ± 0.2	9.9 ± 0.5
7_{-2}–6_{-2}	338722.898	83.0148	15.7	12.53 ± 0.07	−90.04 ± 0.01	5.61 ± 0.03
[a]18_2–17_3	344109.039	411.5062	6.79	…	…	…

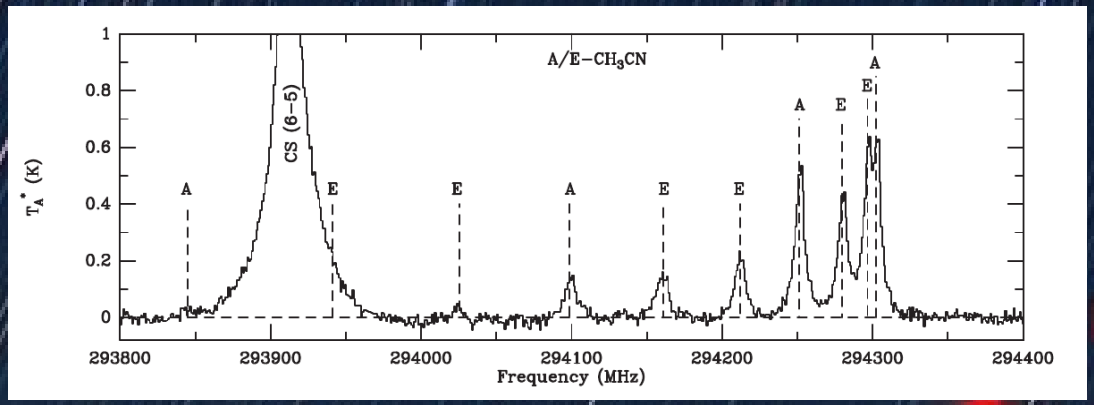

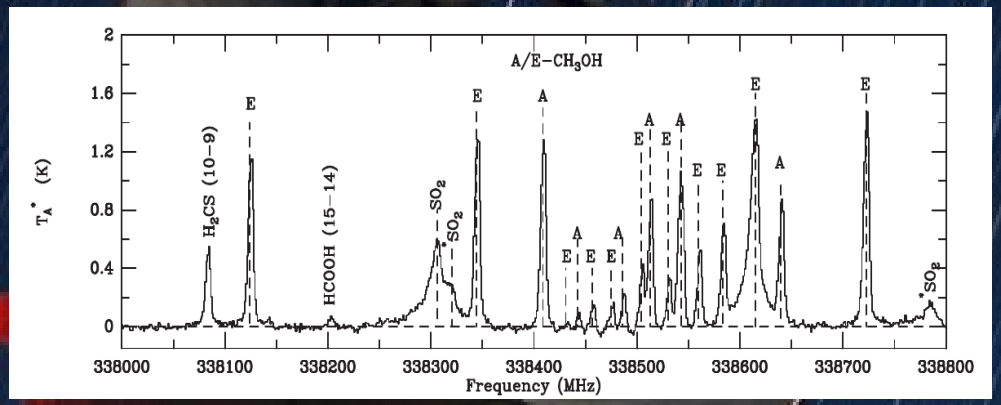

Science with LLAMA. September 5-9 2022. Salta, Argentina

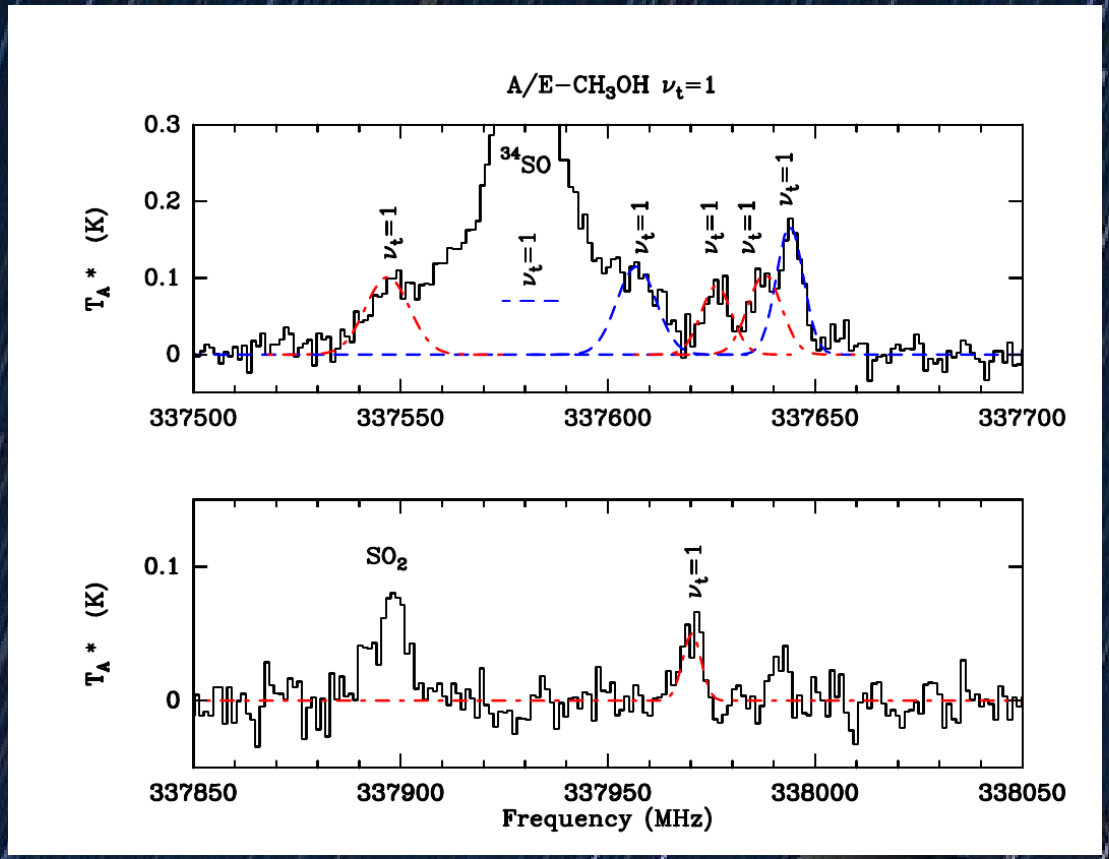

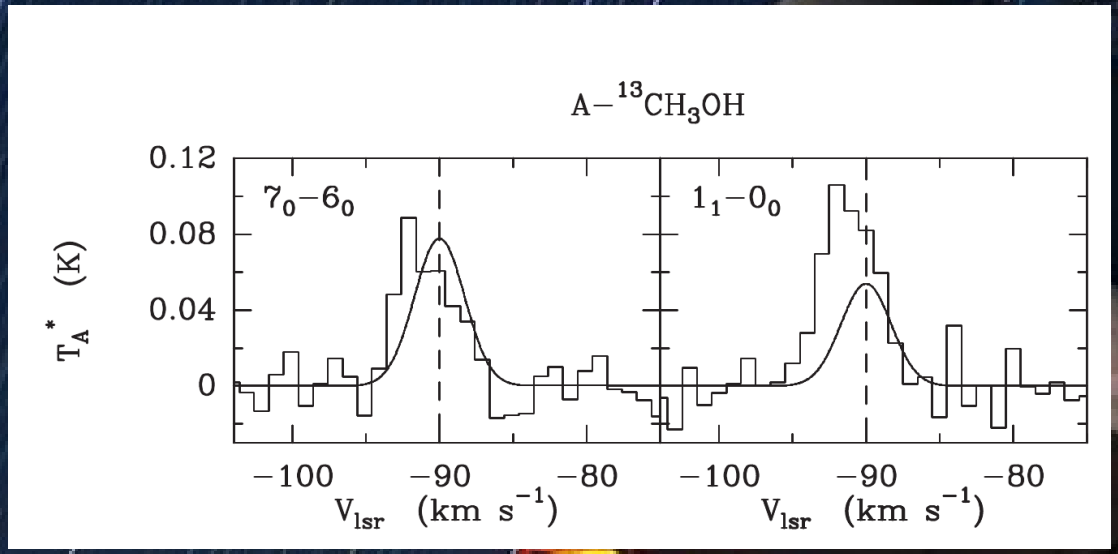

Science with LLAMA. September 5-9 2022. Salta, Argentina

non-LTE

Parameters and Physical Conditions Derived from the Statistical Equilibrium Calculations that have Yielded Hydrogen Densities between 0.7 and 1×10^7 cm^{-3}

Parameters	A–CH_3CN	E–CH_3CN	A–CH_3OH	E–CH_3OH
Modeled lines	7	13	10	13
χ^2 min	5.69	7.77	6.23	4.42
FWHM (km s^{-1})	5.49 ± 0.01	5.49 ± 0.01	4.9 ± 0.1	4.88 ± 0.01
N (10^{14} cm^{-2})	4.77 ± 0.05	3.69 ± 0.04	85 ± 20	98 ± 0.1
T_k (K)	142.1 ± 0.9	140.5 ± 0.3	64 ± 2	84.8 ± 0.1
θ ($''$)	4.51 ± 0.01	4.53 ± 0.02	5.7 ± 0.3	5.01 ± 0.04

LTE

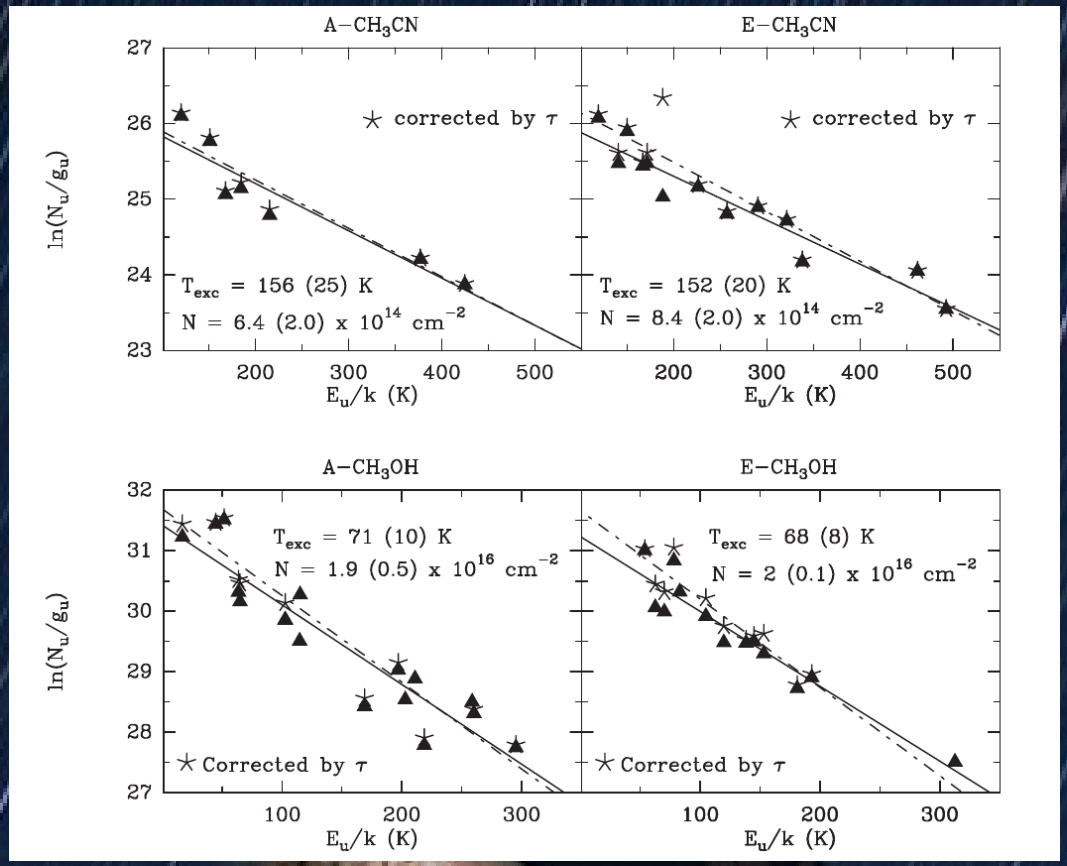

$$[CH_3OH] \approx 8.1 \times 10^{-8}$$

$$[CH_3CN] \approx 3.1 \times 10^{-9}$$

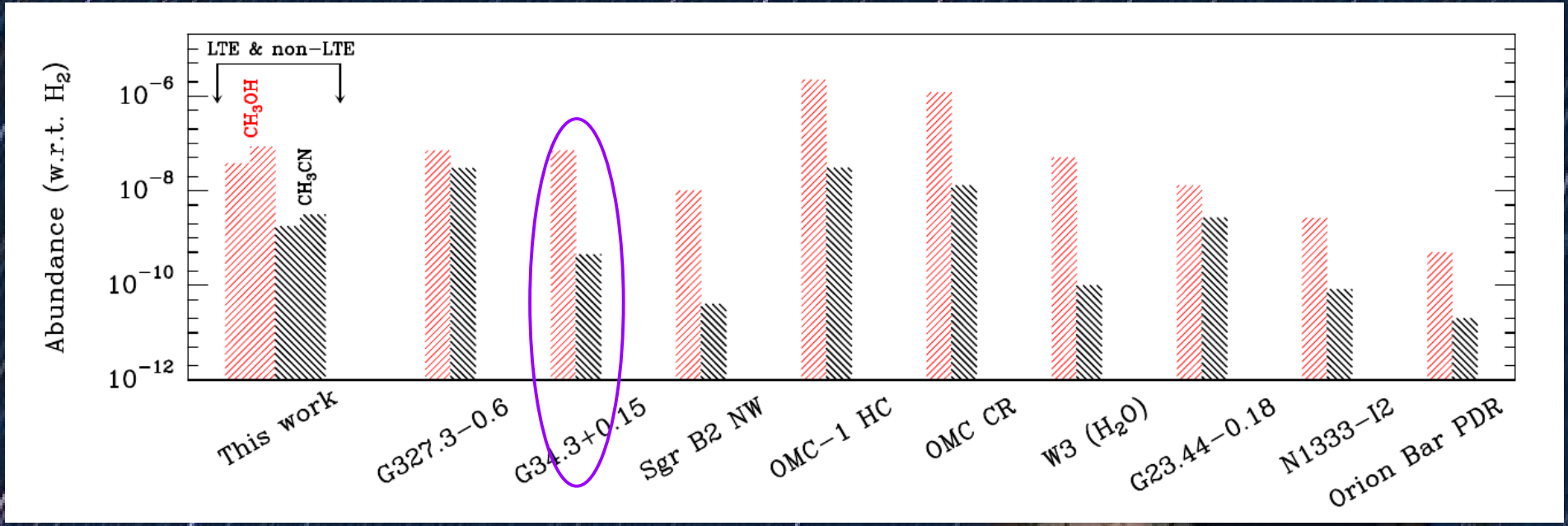

Nomura & Millar (2004) --------- > 10^4 years.

APEX-1

RMS ~ 0.03 K (Ta)
DV = 0.15 km/s

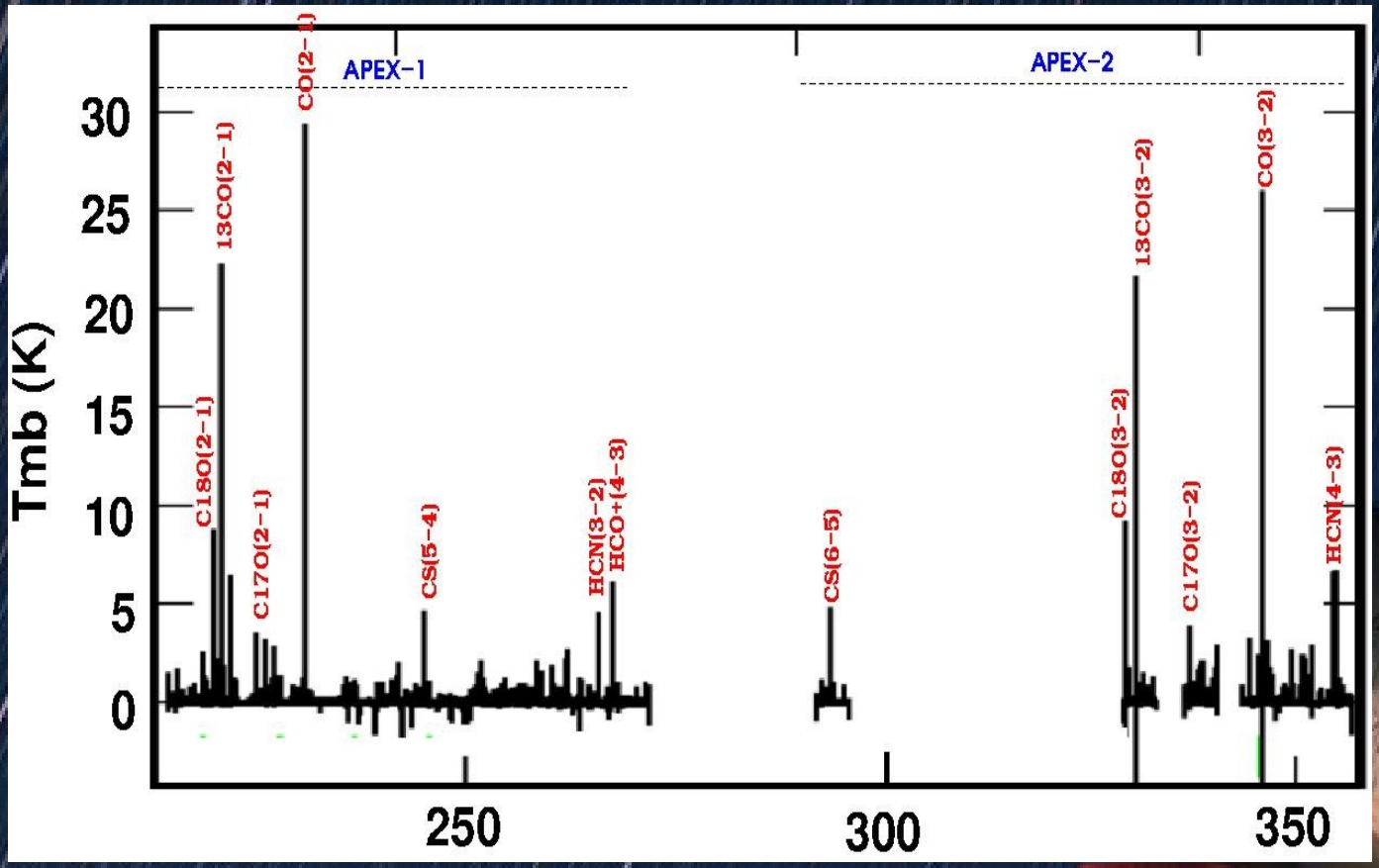

HC_3N $(HC_{(2n+1)}N)$

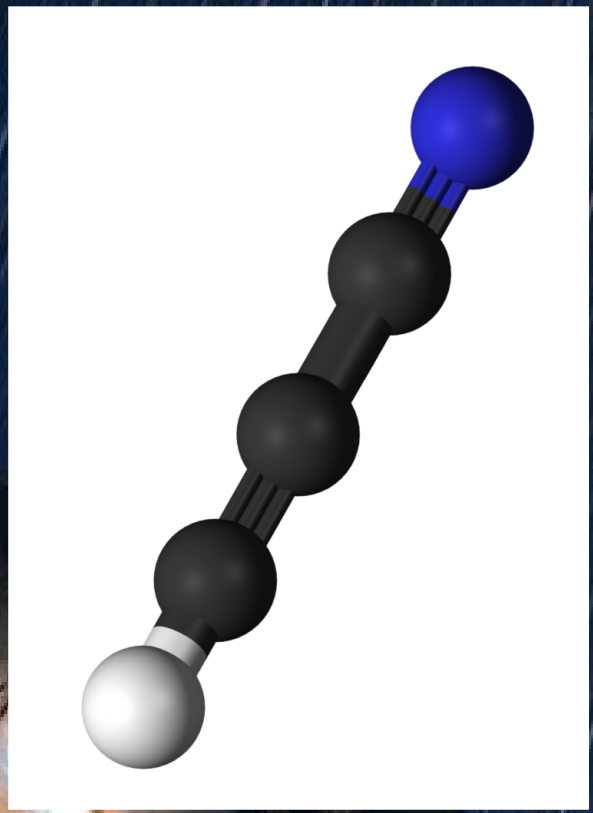

Monthly Notices of the ROYAL ASTRONOMICAL SOCIETY

MNRAS **00,** 1 (2019)
Advance Access publication 2019 July 31

doi:10.1093/mnras/stz2087

Cyanoacetylene in the outflow/hot molecular core G331.512−0.103

N. U. Duronea,[1★] L. Bronfman,[2] E. Mendoza,[3] M. Merello,[3] R. Finger,[2] N. Reyes,[2,4] C. Hervías-Caimapo,[5] A. Faure,[6] C. E. Cappa,[7] E. M. Arnal,[7] J. R. D. Lépine,[3] I. Kleiner[8] and L-Å. Nyman[9]

[1] *Instituto Argentino de Radioastronomía, CONICET, CCT-La Plata, C.C.5., 1894, Villa Elisa, and CIC, Prov. de Bs. As. Argentina*
[2] *Departamento de Astronomía, Universidad de Chile, Casilla 36, Santiago de Chile*
[3] *Instituto de Astronomia, Geofísica e Ciências Atmosféricas, Universidad de São Pãulo, São Pãulo SP-05508-090, Brazil*
[4] *Departamento de Ingeniería Eléctrica, Universidad de Chile, Santiago de Chile*
[5] *Department of Physics, Florida State University, Tallahassee, FL 32306, USA*
[6] *Université Grenoble Alpes, CNRS, IPAG, F-38000 Grenoble, France*
[7] *Facultad de Ciencias Astronómicas y Geofísicas, Universidad Nacional de La Plata, Paseo del Bosque s/n, 1900 La Plata, Argentina*
[8] *Laboratoire Interuniversitaire des Systemes Atmospheriques (LISA), CNRS, UMR 7583, Université de Paris-Est Créteil et Paris Diderot, 61, Av Général de Gaulle, F-94010 Créteil Cedex, France*
[9] *Joint ALMA Observatory, JAO Alonso de Córdova 31070, Vitacura, Santiago de Chile, Chile*

Accepted 2019 July 18. Received 2019 July 12; in original form 2019 April 26

ABSTRACT

Using APEX-1 and APEX-2 observations, we have detected and studied the rotational lines of the HC_3N molecule (cyanoacetylene) in the powerful outflow/hot molecular core G331.512−0.103. We identified 31 rotational lines at J levels between 24 and 39; 17 of them in the ground vibrational state $v = 0$ (9 lines corresponding to the main C isotopologue and 8 lines corresponding to the ^{13}C isotopologues), and 14 in the lowest vibrationally excited state $v_7 = 1$. Using local thermodynamic equilibrium (LTE)-based population diagrams for the beam-diluted $v = 0$ transitions, we determined $T_{exc} = 85 \pm 4$ K and $N(HC_3N) = (6.9 \pm 0.8) \times 10^{14}$ cm^{-2}, while for the beam-diluted $v_7 = 1$ transitions we obtained $T_{exc} = 89 \pm 10$ K and $N(HC_3N) = (2 \pm 1) \times 10^{15}$ cm^{-2}. Non-LTE calculations using H_2 collision rates indicate that the HC_3N emission is in good agreement with LTE-based results. From the non-LTE method, we estimated $T_{kin} \simeq 90$ K, $n(H_2) \simeq 2 \times 10^7$ cm^{-3} for a central core of 6 arcsec in size. A vibrational temperature in the range from 130 to 145 K was also determined, values which are very likely lower limits. Our results suggest that rotational transitions are thermalized, while infrared radiative pumping processes are probably more efficient than collisions in exciting the molecule to the vibrationally excited state $v_7 = 1$. Abundance ratios derived under LTE conditions for the ^{13}C isotopologues suggest that the main formation pathway of HC_3N is $C_2H_2 + CN \rightarrow HC_3N + H$.

Key words: astrochemistry – stars: formation – ISM: abundances – ISM: individual objects: – ISM: jets and outflows.

1 INTRODUCTION

Cyanopolyynes molecules ($HC_{2n+1}N$, $n \geq 1$) are typical carbon-chain molecules that seem to be ubiquitous in the interstellar medium (ISM) since they have been detected in a wide range of environments both in the Milky Way and in other galaxies. The shortest member of the family, HC_3N (cyanoacetylene), is the most abundant cyanopolyyne. Due to its low rotational constant (1/13 of CO) and large dipole moment (3.7 D, DeLeon & Muenter 1985), cyanoacetylene lines can be detected over a wide range of rotational lines (closely spaced by only 9.1 GHz) at relatively low frequencies, in contrast with, for example, HCN or HCO^+, which have high-J lines at very high frequencies that are extremely difficult to detect with ground-based telescopes. The critical density of HC_3N ($n_{H_2} \sim 10^5$–10^6 cm^{-3}) is comparable to other high-density gas tracers, such as HCN, CS, or HCO^+. In addition, HC_3N is usually optically thin even in low-J transitions, mostly due to its relatively low abundance, which is suitable for studying dense molecular gas (e.g. Bergin, Snell & Goldsmith 1996). This makes it easier to conduct multitransition analysis for HC_3N than for other dense molecular gas tracers, which can help to better understand the

★ E-mail: duronea@iar.unlp.edu.ar

© 2019 The Author(s)
Published by Oxford University Press on behalf of the Royal Astronomical Society

Table 1. HC_3N lines detected in G331 and their parameters obtained from Gaussian fits.

Transition	Frequency (MHz)	E_u (K)	A_{ul} ($\times 10^{-5}s^{-1}$)	$\int T_{mb}\, dv$ (K km s^{-1})	V_{lsr} (km s^{-1})	T_{peak} (K)	FWHM (km s^{-1})	τ	Remark§
$v = 0$									
24–23	218324.72	130.98	82.6	6.94 ± 0.72	-90.35 ± 0.05	1.17 ± 0.05	5.39 ± 0.11	0.298*	cl
25–24	227418.91	141.89	93.5	7.49 ± 0.75	-90.37 ± 0.05	1.23 ± 0.05	5.57 ± 0.11	0.278*	cl
26–25	236512.78	153.24	105.2	6.20 ± 0.62	-90.35 ± 0.05	0.99 ± 0.04	5.55 ± 0.12	0.260*	cl
27–26	245606.31	165.03	117.9	6.02 ± 0.61	-90.37 ± 0.07	0.94 ± 0.06	5.63 ± 0.17	0.248*	cl
28–27	254699.51	177.25	131.6	6.47 ± 0.66	-90.37 ± 0.07	1.02 ± 0.06	5.58 ± 0.15	0.235*	pbw $^{33}SO_2$ nl CH_2NH
29–28	263792.31	189.91	146.3	5.85 ± 0.59	-90.49 ± 0.07	0.89 ± 0.06	5.93 ± 0.16	0.206*	pbw CH_3OH
37–36	336520.08	306.91	304.8	4.86 ± 0.50	-90.50 ± 0.08	0.65 ± 0.05	6.67 ± 0.19	0.082*	nl SO
38–37	345609.01	323.49	330.2	3.87 ± 0.39	-90.57 ± 0.06	0.58 ± 0.04	6.16 ± 0.14	0.077*	pbw CH_3OH
39–38	354697.46	340.51	357.1	4.14 ± 0.43	-90.54 ± 0.08	0.53 ± 0.04	6.92 ± 0.18	0.060*	cl
^{13}C Isotopologues									
$H^{13}CCCN$									
26–25	229203.09	148.51	95.7	0.28 ± 0.04	-91.1 ± 0.2	0.06 ± 0.02	4.1 ± 0.4	0.024†	cl
27–26	238015.68	159.93	197.3	0.30 ± 0.04	-90.9 ± 0.2	0.06 ± 0.02	4.8 ± 0.5	0.022†	cl
$HC^{13}CCN$									
24–23	217398.56	130.42	81.5	0.28 ± 0.05	-89.4 ± 0.4	0.07 ± 0.02	4.2 ± 0.8	0.025†	cl
25–24	226454.18	141.29	92.3	0.32 ± 0.05	-90.7 ± 0.4	0.06 ± 0.02	5.9 ± 1.0	0.024†	cl
27–26	244564.44	164.33	116.4	0.32 ± 0.06	-91.5 ± 0.4	0.07 ± 0.03	3.6 ± 0.8	0.027†	pbw CH_3OH
$HCC^{13}CN$									
24–23	217419.57	130.44	81.6	0.51 ± 0.06	-90.2 ± 0.2	0.10 ± 0.02	5.4 ± 0.4	0.035†	pbw CH_3OH nl ^{13}CN
25–24	226476.04	141.31	92.3	0.43 ± 0.06	-89.9 ± 0.4	0.08 ± 0.03	5.4 ± 0.7	0.031†	cl
26–25	235532.20	152.61	103.9	0.50 ± 0.07	-88.9 ± 0.3	0.09 ± 0.02	5.6 ± 0.6	0.037†	cl
$v_7 = 1$									
24_{-1}–23_1	218860.81	452.15	82.7	0.58 ± 0.07	-91.3 ± 0.3	0.10 ± 0.03	4.9 ± 0.5	0.015*	cl
24_1–23_{-1}	219173.75	452.34	83.0	0.34 ± 0.05	-91.6 ± 0.3	0.08 ± 0.02	4.1 ± 0.6	0.018*	cl
25_1–24_{-1}	227977.27	463.09	93.5	0.69 ± 0.08	-90.2 ± 0.2	0.12 ± 0.02	6.0 ± 0.5	0.013*	cl
25_{-1}–24_1	228303.17	463.29	93.4	0.70 ± 0.09	-90.8 ± 0.3	0.10 ± 0.02	6.8 ± 0.6	0.011*	cl
26_{-1}–25_1	237093.38	474.47	105.2	0.53 ± 0.07	-90.5 ± 0.4	0.07 ± 0.02	8.4 ± 1.2	0.009*	cl
26_1–25_{-1}	237432.26	474.69	105.7	0.57 ± 0.07	-91.0 ± 0.2	0.10 ± 0.03	5.3 ± 0.5	0.014*	cl
27_1–26_{-1}	246209.14	486.29	118.0	0.45 ± 0.08	-91.4 ± 0.5	0.07 ± 0.03	9.0 ± 1.9	0.011*	cl
27_{-1}–26_1	246560.95	486.52	118.5	0.78 ± 0.10	-89.3 ± 0.4	0.10 ± 0.03	8.1 ± 0.9	0.009*	cl
28_{-1}–27_1	255324.55	498.54	131.7	0.58 ± 0.10	-91.5 ± 0.5	0.09 ± 0.03	6.7 ± 1.1	0.011*	cl
28_1–27_{-1}	255689.29	498.79	132.2	0.72 ± 0.11	-91.3 ± 0.6	0.08 ± 0.02	8.9 ± 1.6	0.008*	cl
29_1–28_{-1}	264439.58	511.23	146.4	0.20 ± 0.04	-91.6 ± 0.3	0.05 ± 0.03	2.6 ± 0.7	0.029*	cl
29_{-1}–28_1	264817.24	511.50	147.1	0.40 ± 0.07	-91.1 ± 0.5	0.07 ± 0.02	6.2 ± 1.1	0.012*	cl
32_1–31_{-1}	292198.64	552.26	197.9	0.50 ± 0.08	-90.2 ± 0.3	0.09 ± 0.02	4.9 ± 0.6	0.014*	cl
39_{-1}–38_1	356072.44	662.68	359.2	0.31 ± 0.06	-90.3 ± 0.4	0.05 ± 0.02	6.6 ± 1.0	0.008*	nlo SO_2

*Obtained iteratively from the opacity correction (Sect 4.2.1) †Obtained from Eq.8 (Sect. 4.2.3)

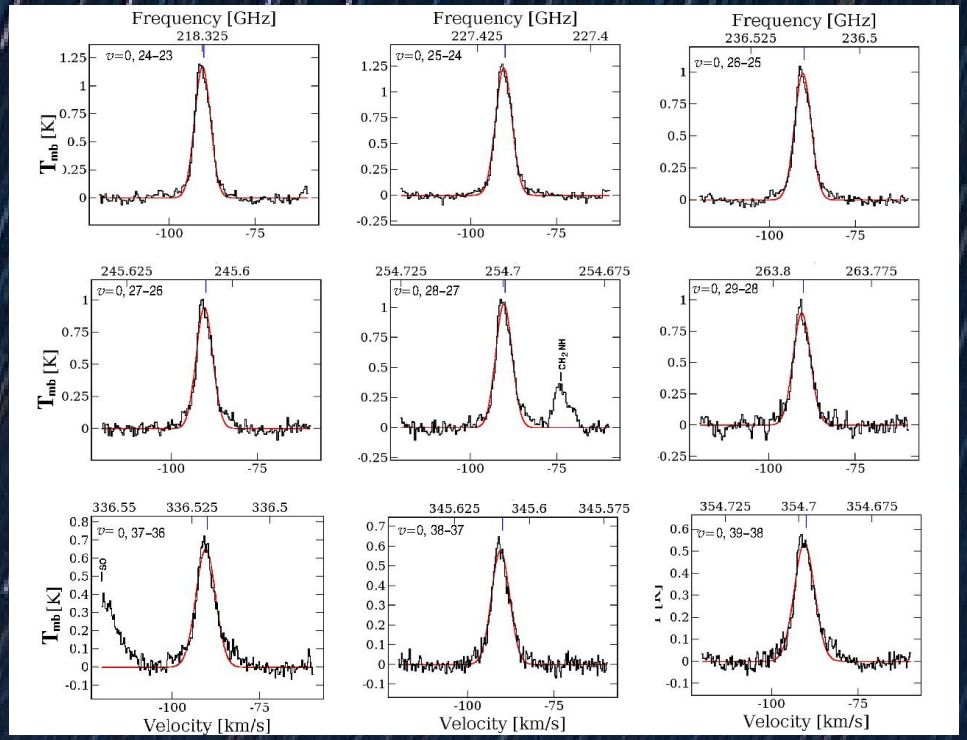

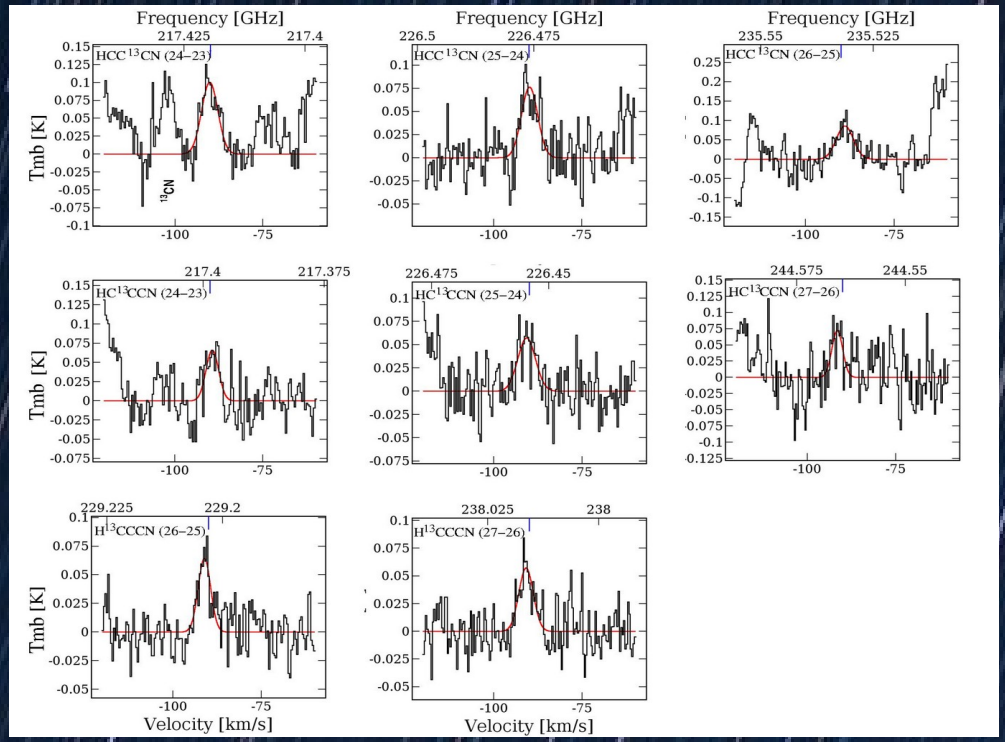

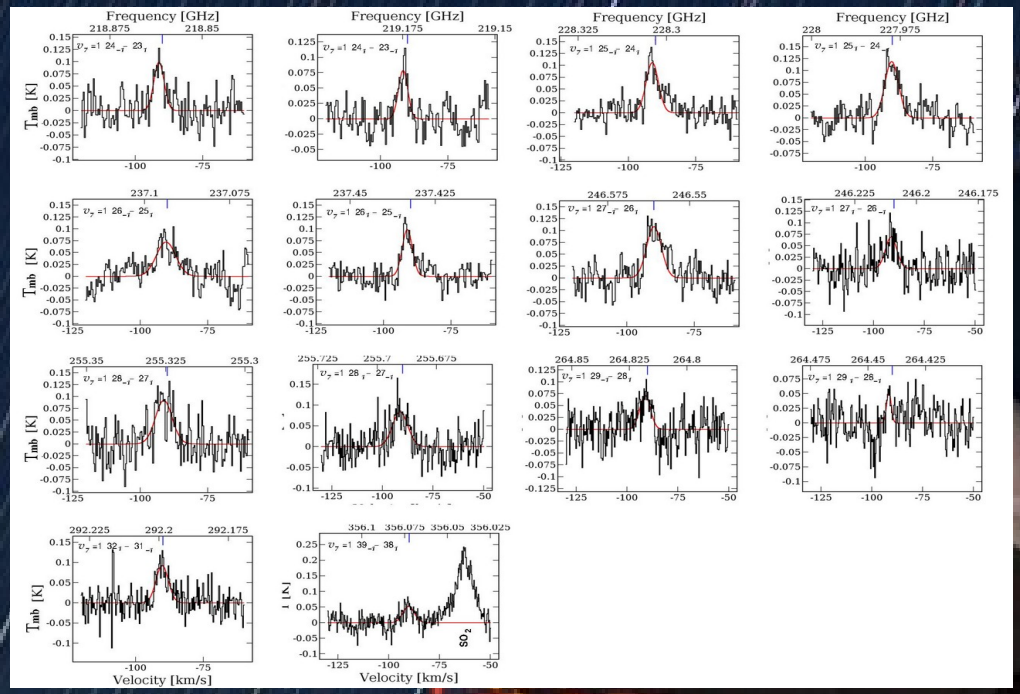

Science with LLAMA. September 5-9 2022. Salta, Argentina

LTE

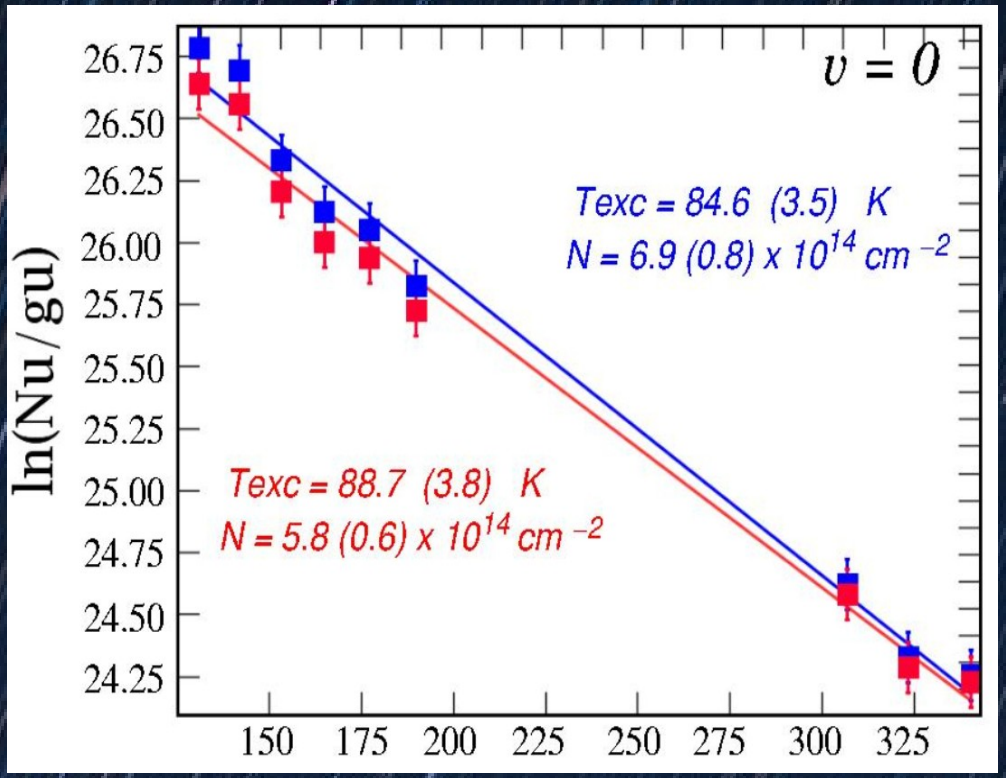

non-LTE

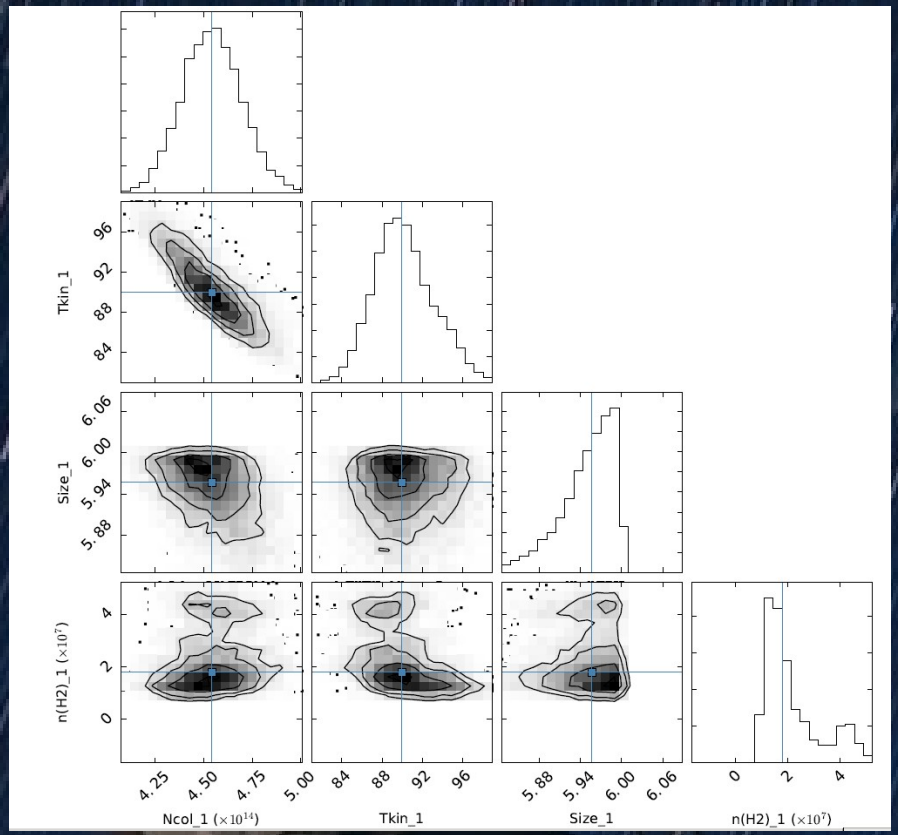

N(HC3N)=4.5x10^{14} cm^{-2}
Tkin= 90 K
n(H2)=2x10^{7} cm^{-3}
(size <= 6”)

Excitation of the v=0 and v_7=1 lines

$$n_c^{J,J-1} \approx \frac{A_{(J,J-1)}}{\gamma(J,J-1)}$$

J=38-37 n_c (80-100 K) ~ 1.5 x 10^7 cm^{-3}
n(RADEX)~2 x 10^7 cm^{-3}
→ rotational transitions v=0 in LTE

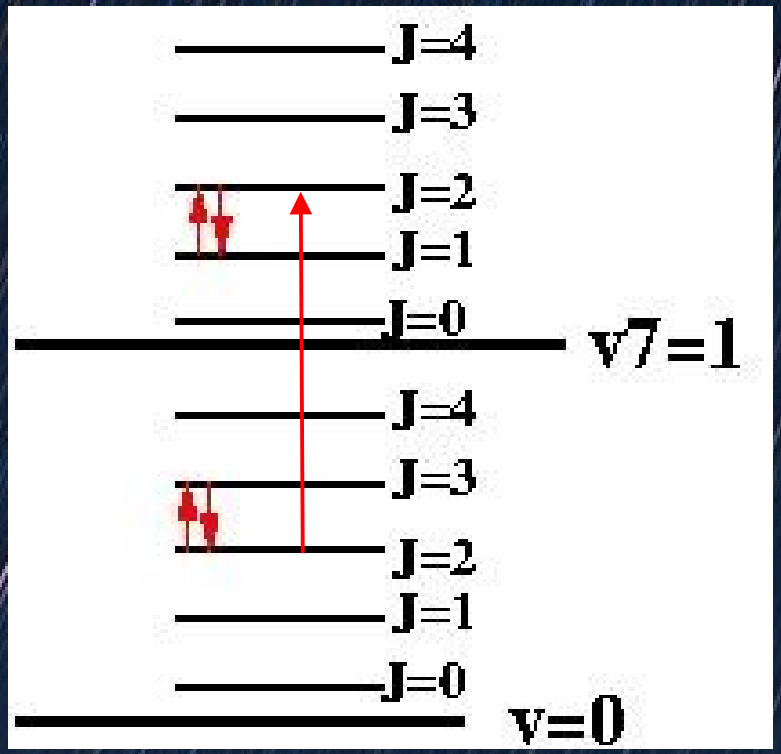

n_c (v_7=1-0) ~ 4 x 10^8 cm^{-3} (Wyrowski et al., 1999)

→ IR pumping (dust)

$$\frac{W_{(v_7=1)}}{W_{(v=0)}} = \exp\left(\frac{-\Delta E_{70}}{kT_{\rm vib}}\right)$$

Tvib = 140 K → Tdust

$$\frac{L_{\rm hc}}{L_\odot} = 1.8625 \times 10^{-5} \left(\frac{r}{10^{16}\ {\rm cm}}\right)^2 T_{\rm dust}^4$$

→ *O4 (ZAMS)*

Isotopologue	N [$\times 10^{13}$ cm^{-2}]	X [$\times 10^{-11}$]	$^{12}C/^{13}C$
HC_3N	$69 \pm 8^{\dagger}$	79 – 62	-
$HCC^{13}CN$	6.7 ± 0.9	7.8 – 5.9	~ 10
$HC^{13}CCN$	3.8 ± 0.8	4.7 – 3.1	~ 18
$H^{13}CCCN$	3.7 ± 0.6	4.4 – 3.2	~ 19
$^{13}C\ HC_3N$	$3.3 \pm 0.2^{\ddagger}$	3.6 – 3.2	~ 21

$$[HCC^{13}CN]:[HC^{13}CCN]:[H^{13}CCCN] = 1.8(\pm 0.5):1.0:1.0(\pm 0.4)$$

$$C_2H_2 + CN \longrightarrow HCCCN + H$$

$$H_2C_2 + {}^{13}CN \longrightarrow HCC^{13}CN + H$$

$$\downarrow$$

$$[HCC^{13}CN]:[HC^{13}CCN]:[H^{13}CCCN] = a:b:c, \text{ with } a>b\approx c$$

SEPIA

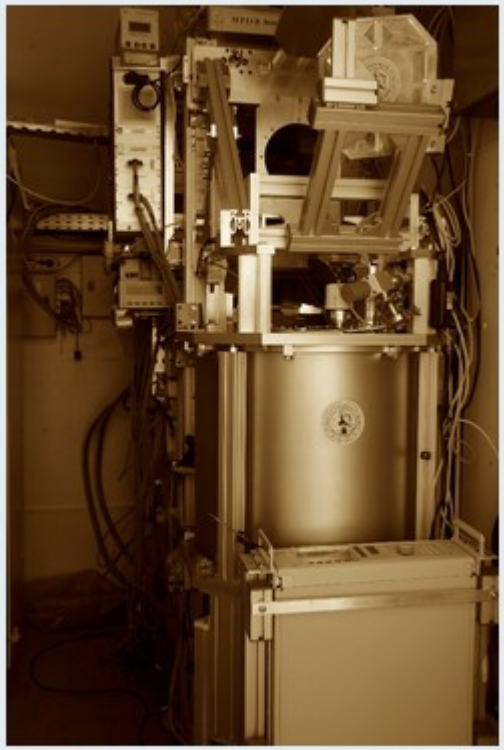

- SEPIA660 covering the window 597 – 725 GHz
- SEPIA345 covering the window 272 – 376 GHz
- SEPIA180 covering the window 159 – 211 GHz

Instrumento (FE/BE)	Tipo	Frec [GHz]	HPBW (arcsec)	Rango IF [GHz]	Elementos	Pol
SEPIA180 FFTS1	Heterodino SIS (2SB)	157-211	39-31	4-8	1	Dual

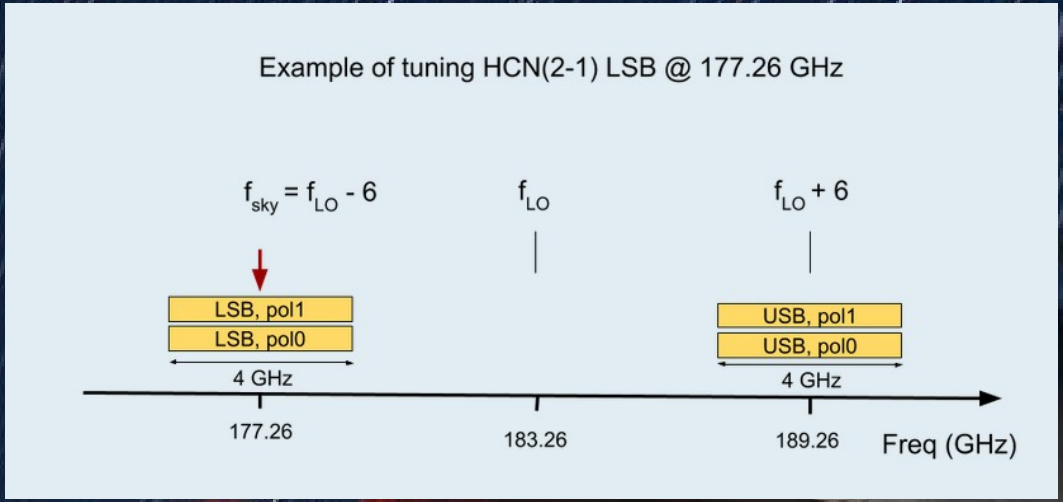

HNCO

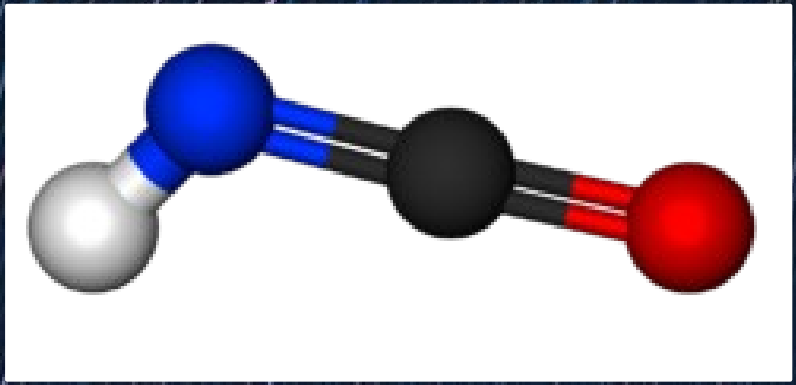

MNRAS **000**, 1–17 (2020) Preprint 22 April 2021 Compiled using MNRAS LaTeX style file v3.0

Isocyanic acid (HNCO) in the Hot Molecular Core G331.512-0.103: Observations and Chemical Modelling

Carla M. Canelo,[1★] Leonardo Bronfman,[2] Edgar Mendoza,[1,3] Nicolas Duronea,[4] Manuel Merello,[2] Miguel Carvajal,[5,6] Amâncio C.S. Friaça,[1] and Jacques Lepine[1]

[1]*Departamento de Astronomia, Instituto de Astronomia, Geofísica e Ciências Atmosféricas, Universidade de São Paulo, São Paulo, Brazil*
[2]*Departamento de Astronomía, Universidad de Chile, Casilla 36-D, Santiago de Chile, Chile*
[3]*Observatório do Valongo, Universidade Federal do Rio de Janeiro, Ladeira Pedro Antônio, 43, Rio de Janeiro – RJ 20.080-090, Brazil*
[4]*Instituto de Astrofísica de La Plata (UNLP - CONICET), La Plata, Argentina*
[5]*Dept. Ciencias Integradas, Facultad de Ciencias Experimentales, Centro de Estudios Avanzados en Física, Matemática y Computación, Unidad Asociada GIFMAN, CSIC-UHU, Universidad de Huelva, Spain*
[6]*Instituto Universitario Carlos I de Física Teórica y Computacional, Universidad de Granada, Spain*

arXiv:2104.10605v1 [astro-ph.GA] 21 Apr 2021

Accepted 2021 April 20. Received 2021 April 20; in original form 2021 January 27.

ABSTRACT

Isocyanic acid (HNCO) is a simple molecule with a potential to form prebiotic and complex organic species. Using a spectral survey collected with the Atacama Pathfinder EXperiment (APEX), in this work we report the detection of 42 transitions of HNCO in the hot molecular core/outflow G331.512-0.103 (hereafter G331). The spectral lines were observed in the frequency interval ~ 160–355 GHz. By means of Local Thermodynamic Equilibrium (LTE) analyses, applying the rotational diagram method, we studied the excitation conditions of HNCO. The excitation temperature and column density are estimated to be T_{ex}= 58.8 ± 2.7 K and $N = (3.7 \pm 0.5) \times 10^{15}$ cm^{-2}, considering beam dilution effects. The derived relative abundance is between (3.8 ± 0.5) $\times 10^{-9}$ and (1.4 ± 0.2) $\times 10^{-8}$. In comparison with other hot molecular cores, our column densities and abundances are in agreement. An update of the internal partition functions of the four CHNO isomers: HNCO; cyanic acid, HOCN; fulminic acid, HCNO; and isofulminic acid, HONC is provided. We also used the astrochemical code Nautilus to model and discuss HNCO abundances. The simulations could reproduce the abundances with a simple zero-dimensional model at a temperature of 60 K and for a chemical age of ~10^5 years, which is larger than the estimated dynamical age for G331. This result could suggest the need for a more robust model and even the revision of chemical reactions associated with HNCO.

Key words: ISM: molecules – astrochemistry – methods: observational – molecular data – molecular processes

1 INTRODUCTION

The isocyanic acid (HNCO) is the simplest molecule containing four of the six biogenic elements: carbon, hydrogen, oxygen, nitrogen, phosphorus and sulphur (abbreviated as CHONPS) that are present in all living beings. Although it has only four atoms, HNCO could be precursor of other prebiotic and complex organic molecules (COMs[1]), which are of great astrochemical and astrobiological interest due to their potential to form molecules such as amino acids, sugars and nucleobases (e.g. Gorai et al. 2020, and references therein). HNCO molecules are included as a peptide bond [–(H)N–C(O)–] between any two single amino acid, such as glycine (Fedoseev et al. 2015). Moreover, recent experiments, simulating interstellar ice chemical processes, have shown that HNCO and CH_4 can form molecules with peptide bonds in solid state under far-UV irradiation (Ligterink et al. 2018). The observation of COMs in astrophysical environments, along with the study of their formation and destruction pathways, are important for a better comprehension of the origins of life on Earth and elsewhere.

The potential interest of HNCO in radio astronomy has generated and stimulated debates, specially about its formation and detection. Among the first experimental works, Jones et al. (1950) and Jones & Badger (1950) made experimental investigations of the infrared and microwave spectra of HNCO and HNCS. Hocking et al. (1972) and Hocking et al. (1975) carried out laboratory measurements to study the HNCO microwave and millimeter spectrum. Concurrently, Snyder & Buhl (1972) reported the results of a survey for HNCO in Galactic molecular sources, concluding about its detection in Sgr B2. HNCO is a near prolate asymmetric top molecule with a linearity barrier at 1899 cm^{-1} (Niedenhoff et al. 1995); its rotational levels undergo a hyperfine splitting caused by the nuclear spin of nitrogen (Lapinov et al. 2007). The rotational levels of HNCO are assigned by the spectroscopic notation for the asymmetric top, such as J_{K_a,K_c}, where J is the rotational angular momentum, and K_a and K_c are the projections of J to the molecule fixed principal a and c-axes, respectively (Hocking et al. 1974; Niedenhoff et al. 1995; Zinchenko et al. 2000).

Churchwell et al. (1986) found that the most likely excitation mechanism of HNCO in Sgr B2 might be radiative rather than collisional,

★ E-mail: camcanelo@gmail.com

[1] As discussed in Herbst & van Dishoeck (2009), the term complex is labelled by astronomers if not by chemist, and makes a reference to interstellar molecules with 6 or more atoms including the element carbon.

© 2020 The Authors

Frequency (MHz)	Transition $(J_{k_a,k_c})_u - (J_{k_a,k_c})_l$	A_{ul} (10^{-5} s^{-1})	E_u (K)	Integrated Flux (K km s^{-1})	FWHM (km s^{-1})	V_{lsr} (km s^{-1})	NIST reference
175843.695	$8_{0,8} - 7_{0,7}$	7.43	37.98	3.71 ± 0.03	5.91 ± 0.05	-90.23 ± 0.02	—
197821.461	$9_{0,9} - 8_{0,8}$	10.70	47.47	3.63 ± 0.03	5.86 ± 0.07	-90.36 ± 0.03	—
219798.274	$10_{0,10} - 9_{0,9}$	14.70	58.02	4.53 ± 0.05	5.53 ± 0.07	-90.50 ± 0.03	[1]
241774.032	$11_{0,11} - 10_{0,10}$	19.60	69.62	5.35 ± 0.33	5.71 ± 0.44	-90.47 ± 0.17	[3]
263748.625	$12_{0,12} - 11_{0,11}$	25.60	82.28	4.86 ± 0.08	5.95 ± 0.12	-90.66 ± 0.04	[1]
285721.951	$13_{0,13} - 12_{0,12}$	32.60	95.99	7.90 ± 0.10	6.70 ± 0.10	-90.76 ± 0.04	—
307693.905	$14_{0,14} - 13_{0,13}$	40.90	110.76	7.24 ± 0.03	6.07 ± 0.03	-90.56 ± 0.01	—
329664.367	$15_{0,15} - 14_{0,14}$	50.40	126.58	8.02 ± 0.07	6.42 ± 0.08	-90.64 ± 0.03	—
351633.257	$16_{0,16} - 15_{0,15}$	61.30	143.46	6.79 ± 0.06	6.60 ± 0.08	-90.51 ± 0.03	[7]
175189.027	$8_{1,8} - 7_{1,7}$	7.16	81.11	1.01 ± 0.01	5.08 ± 0.07	-90.93 ± 0.03	—
176472.191	$8_{1,7} - 7_{1,6}$	7.31	81.39	0.76 ± 0.01	4.60 ± 0.10	-90.97 ± 0.03	—
197085.416	$9_{1,9} - 8_{1,8}$	10.30	90.57	0.68 ± 0.01	4.42 ± 0.08	-90.99 ± 0.03	—
198528.881	$9_{1,8} - 8_{1,7}$	10.50	90.92	1.01 ± 0.01	5.60 ± 0.10	-90.85 ± 0.04	—
218981.009	$10_{1,10} - 9_{1,9}$	14.20	101.08	1.75 ± 0.05	5.73 ± 0.21	-90.67 ± 0.07	[1]
220584.751	$10_{1,9} - 9_{1,8}$	14.50	101.50	1.73 ± 0.06	6.29 ± 0.31	-90.79 ± 0.10	[2]
240875.727	$11_{1,11} - 10_{1,10}$	19.00	112.64	1.56 ± 0.03	5.48 ± 0.12	-90.91 ± 0.05	[3]
242639.704	$11_{1,10} - 10_{1,9}$	19.50	113.15	1.74 ± 0.04	5.52 ± 0.13	-90.67 ± 0.05	[3]
262769.477	$12_{1,12} - 11_{1,11}$	24.80	125.25	1.80 ± 0.10	5.80 ± 0.50	-90.80 ± 0.20	–
264693.655	$12_{1,11} - 11_{1,10}$	25.40	125.85	1.59 ± 0.04	5.21 ± 0.19	-90.85 ± 0.07	[4]
284662.172	$13_{1,13} - 12_{1,12}$	31.70	138.91	2.13 ± 0.03	5.30 ± 0.10	-90.86 ± 0.04	—
286746.514	$13_{1,12} - 12_{1,11}$	32.40	139.61	2.53 ± 0.02	5.53 ± 0.06	-90.91 ± 0.02	—
306553.733	$14_{1,14} - 13_{1,13}$	39.70	153.62	2.13 ± 0.02	5.91 ± 0.07	-90.86 ± 0.02	–
308798.184	$14_{1,13} - 13_{1,12}$	40.60	154.43	2.74 ± 0.02	5.83 ± 0.07	-90.86 ± 0.02	–
330848.569	$15_{1,14} - 14_{1,13}$	50.10	170.31	4.64 ± 0.05	7.40 ± 0.10	-90.56 ± 0.04	[5]
350333.059	$16_{1,16} - 15_{1,15}$	59.70	186.20	3.24 ± 0.04	5.84 ± 0.09	-90.81 ± 0.03	[6]
352897.581	$16_{1,15} - 15_{1,14}$	61.00	187.25	2.55 ± 0.03	5.25 ± 0.08	-90.81 ± 0.03	—
175791.267	$8_{2,7} - 7_{2,6}$	6.65	208.25	0.37 ± 0.01	7.60 ± 0.30	-92.20 ± 0.10	—
175792.957	$8_{2,6} - 7_{2,5}$	6.65	208.25	0.41 ± 0.03	7.90 ± 0.60	-89.40 ± 0.30	—
197762.939	$9_{2,8} - 8_{2,7}$	9.66	217.74	0.51 ± 0.02	9.10 ± 0.40	-92.50 ± 0.20	—
197765.372	$9_{2,7} - 8_{2,6}$	9.66	217.74	0.52 ± 0.05	9.20 ± 0.40	-88.8 ± 0.10	—
219733.850†	$10_{2,9} - 9_{2,8}$	13.50	228.29	–	–	–	[3]
219737.193†	$10_{2,8} - 9_{2,7}$	13.50	228.29	–	–	–	[3]
241703.852^{a}	$11_{2,10} - 10_{2,9}$	18.10	239.89	–	–	–	—
241708.312	$11_{2,9} - 10_{2,8}$	18.10	239.89	0.67 ± 0.04	4.90 ± 0.40	-91.20 ± 0.10	—
285640.923	$13_{2,12} - 12_{2,11}$	30.40	266.25	0.63 ± 0.05	6.40 ± 0.60	-91.60 ± 0.20	—
285648.301	$13_{2,11} - 12_{2,10}$	30.40	266.25	0.53 ± 0.04	6.20 ± 0.60	-91.30 ± 0.1	—
307607.799	$14_{2,13} - 13_{2,12}$	38.20	281.01	0.64 ± 0.02	7.70 ± 0.40	-91.70 ± 0.1	—
307617.020	$14_{2,12} - 13_{2,11}$	38.20	281.01	0.47 ± 0.02	6.10 ± 0.30	-90.70 ± 0.10	—
329573.452	$15_{2,14} - 14_{2,13}$	47.20	296.83	0.57 ± 0.05	5.50 ± 0.60	-91.30 ± 0.20	—
329584.800	$15_{2,13} - 14_{2,12}$	47.20	296.83	0.64 ± 0.08	7.00 ± 1.00	-90.8 ± 0.30	—
351537.795	$16_{2,15} - 15_{2,14}$	57.50	313.70	0.72 ± 0.07	5.80 ± 0.70	-91.60 ± 0.20	—
351551.573	$16_{2,14} - 15_{2,13}$	57.50	313.70	0.46 ± 0.04	5.70 ± 0.70	-90.80 ± 0.20	—

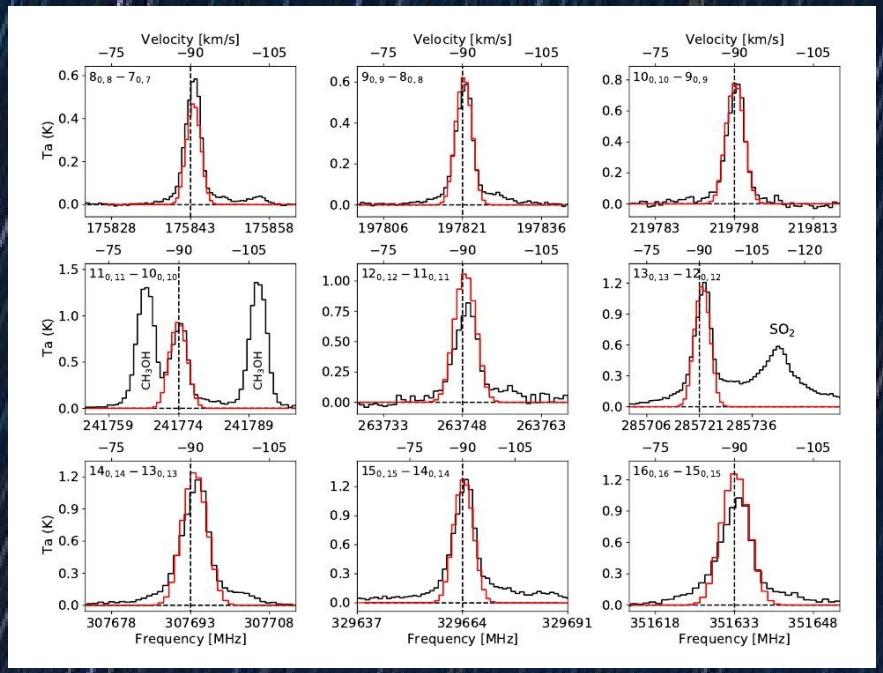

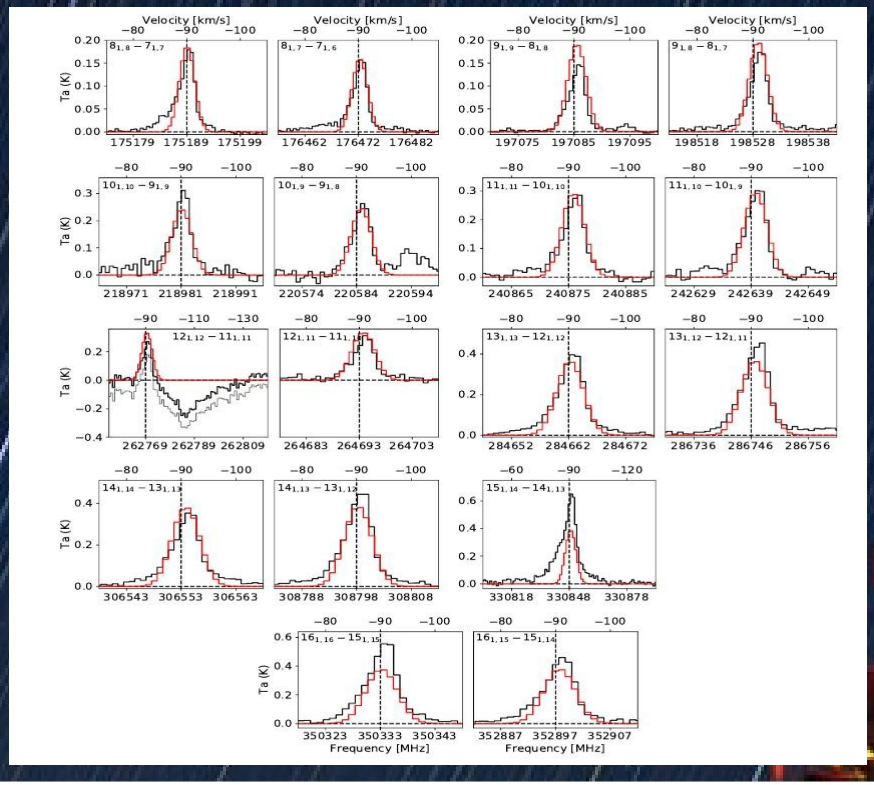

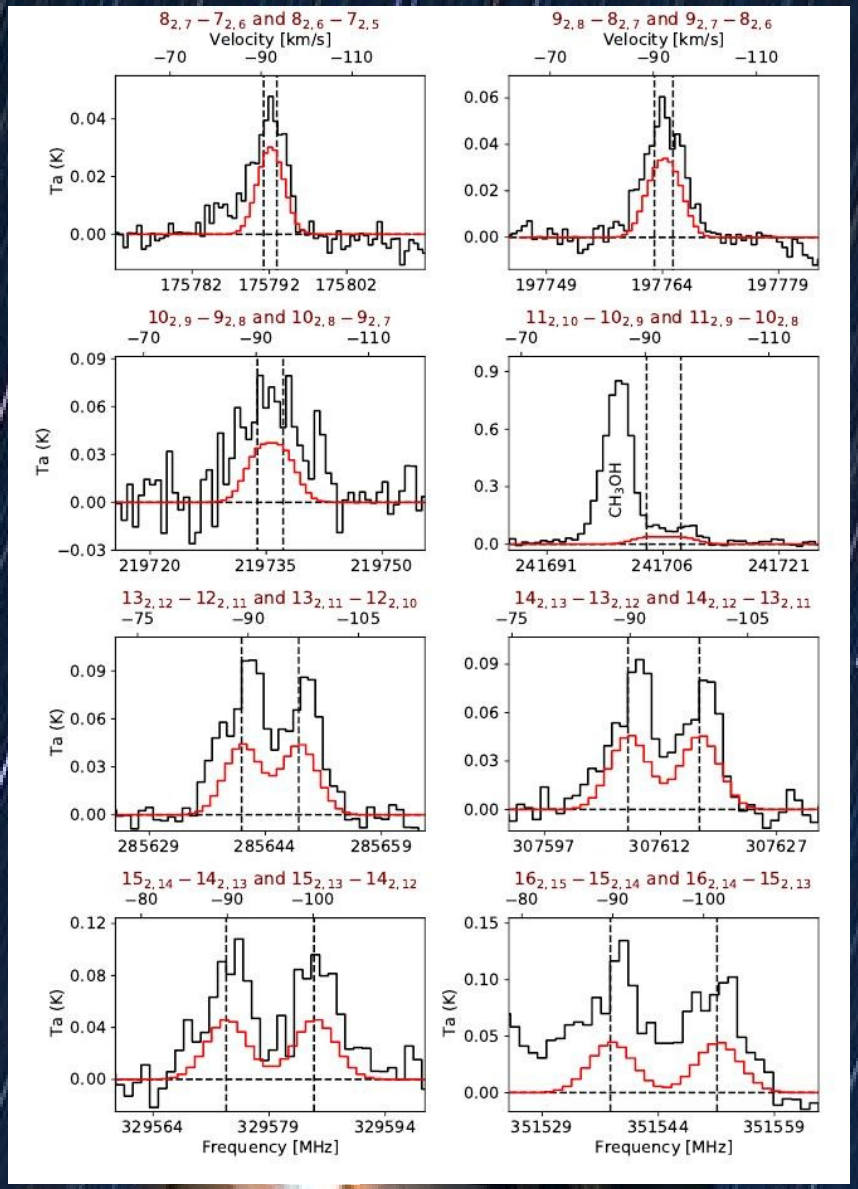

Science with LLAMA. September 5-9 2022. Salta, Argentina

LTE

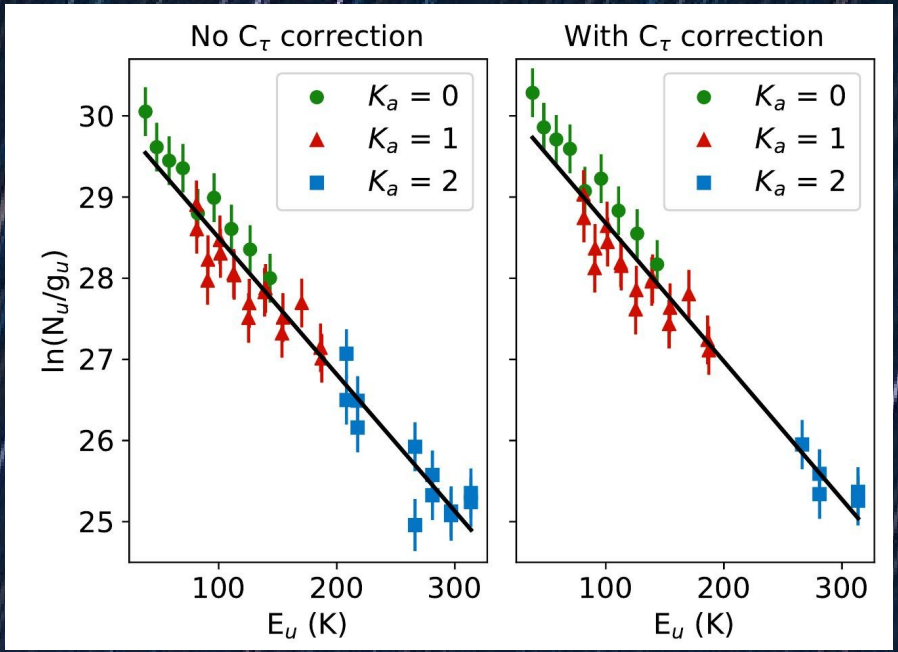

$$N = (3.7 \pm 0.5) \times 10^{15}\ \mathrm{cm}^{-2}$$

$$T_{ex} = 58.8 \pm 2.7\ \mathrm{K}$$

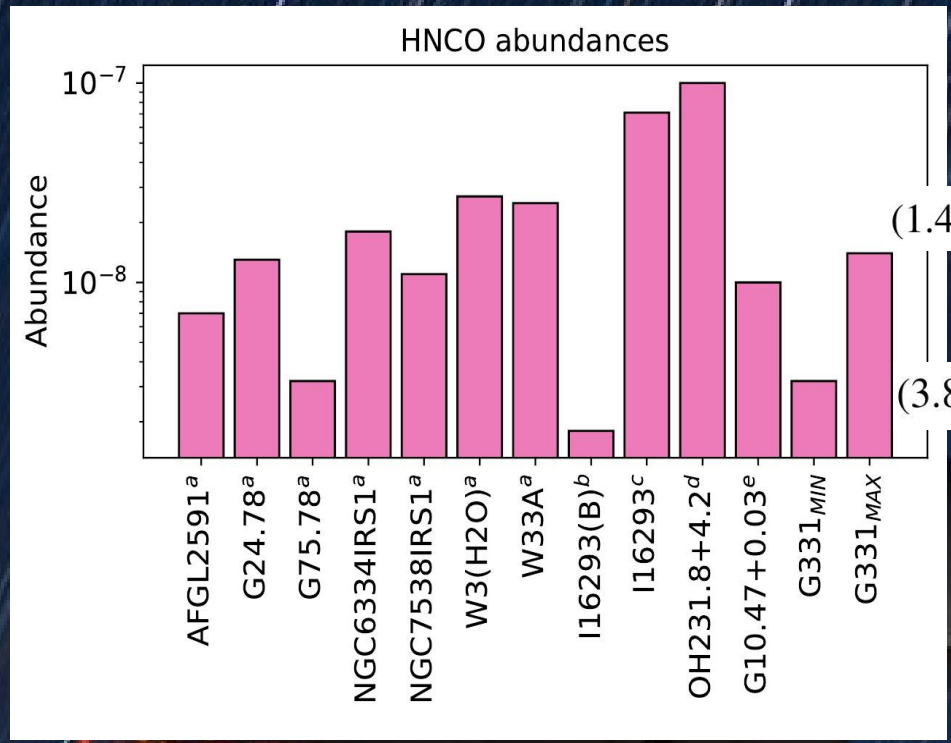

$(1.4 \pm 0.2) \times 10^{-8}$

$(3.8 \pm 0.5) \times 10^{-9}$

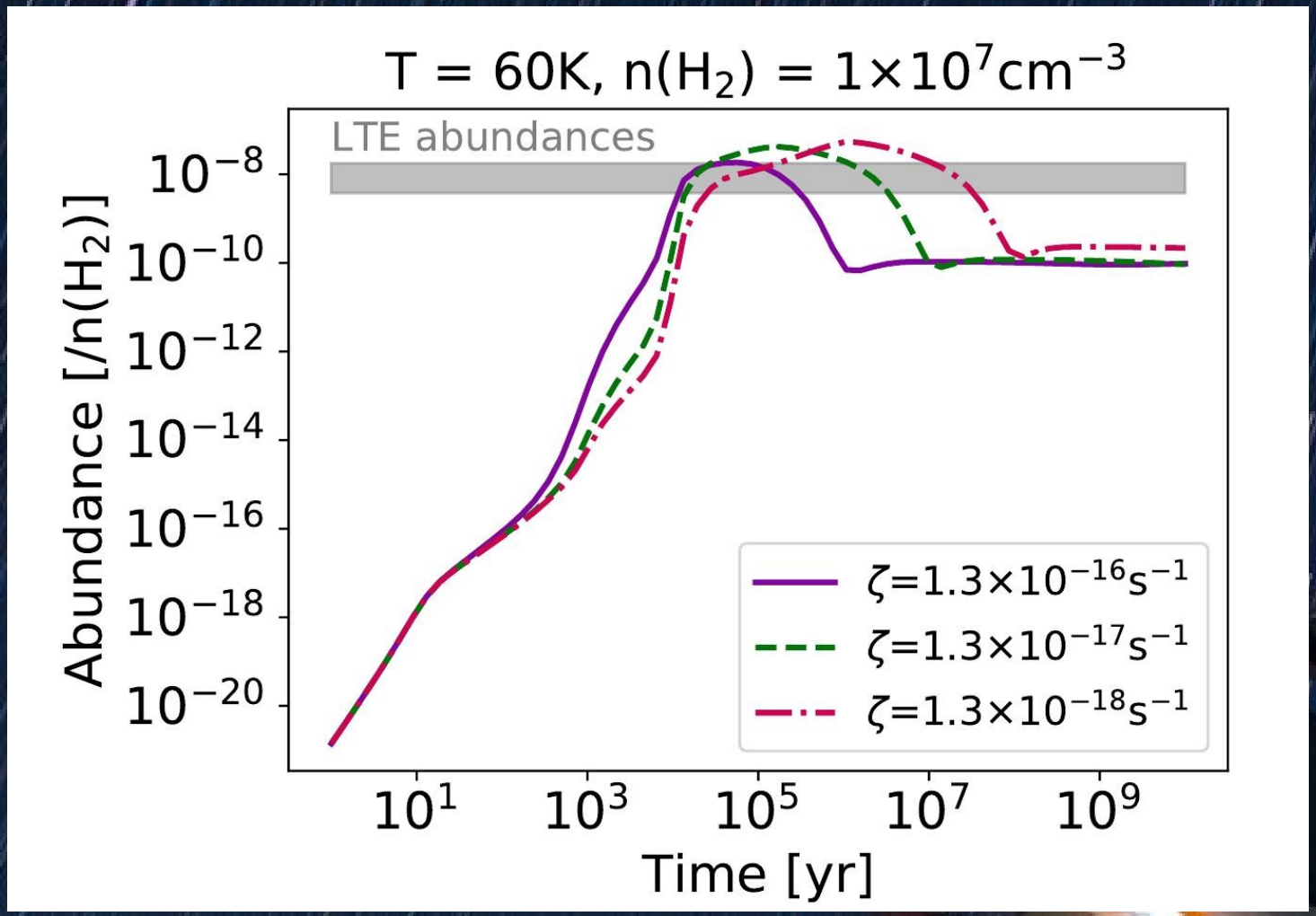
T = 60K, n(H2) = 1×10^7 cm^−3
LTE abundances
Abundance [/n(H2)]
10^−8
10^−10
10^−12
10^−14
10^−16
10^−18
10^−20
10^1
10^3
10^5
10^7
10^9
Time [yr]
ζ=1.3×10^−16 s^−1
ζ=1.3×10^−17 s^−1
ζ=1.3×10^−18 s^−1

The Astrophysical Journal, 925:3 (13pp), 2022 January 20 https://doi.org/10.3847/1538-4357/ac36cc
© 2022. The Author(s). Published by the American Astronomical Society.
OPEN ACCESS

A Spectral Survey of CH_3CCH in the Hot Molecular Core G331.512-0.103

Julia C. Santos[1,2], Leonardo Bronfman[3], Edgar Mendoza[1,4], Jacques R. D. Lépine[1], Nicolas U. Duronea[5,6], Manuel Merello[3], and Ricardo Finger[3]
[1] Instituto de Astronomia, Geofisica e Ciências Atmosféricas; Universidade de São Paulo, Rua do Matão, 1226, São Paulo, SP, Brazil
[2] Laboratory for Astrophysics, Leiden Observatory, Leiden University, P.O. Box 9513, 2300 RA Leiden, The Netherlands; santos@strw.leidenuniv.nl
[3] Departamento de Astronomia; Universidad de Chile, Casilla 36-D, Santiago de Chile, Chile
[4] Observatório do Valongo; Universidade Federal do Rio de Janeiro, Ladeira do Pedro Antônio, 43, Rio de Janeiro, RJ, Brazil
[5] Instituto de Astrofisica de La Plata (UNLP-CONICET), La Plata, Argentina
[6] Faculdad de Ciencias Astronómicas y Geofisicas, Universidad Nacional de La Plata, Paseo del Bosque s/n, 1900, La Plata, Argentina
Received 2021 August 28; revised 2021 November 2; accepted 2021 November 3; published 2022 January 20

Abstract

A spectral survey of methyl acetylene (CH_3CCH) was conducted toward the hot molecular core/outflow G331.512-0.103. Our APEX observations allowed the detection of 41 uncontaminated rotational lines of CH_3CCH in the frequency range between 172 and 356 GHz. Through an analysis under the local thermodynamic equilibrium assumption, by means of rotational diagrams, we determined $T_{exc} = 50 \pm 1$ K, $N(CH_3CCH) = (7.5 \pm 0.4) \times 10^{15}$ cm^2, $X[CH_3CCH/H_2] \approx (0.8\text{–}2.8) \times 10^{-8}$, and $X[CH_3CCH/CH_3OH] \approx 0.42 \pm 0.05$ for an extended emitting region ($\sim 10''$). The relative intensities of the $K = 2$ and $K = 3$ lines within a given K-ladder are strongly negatively correlated to the transitions' upper J quantum number ($r = -0.84$). Pure rotational spectra of CH_3CCH were simulated at different temperatures, in order to interpret this observation. The results indicate that the emission is characterized by a nonnegligible temperature gradient with upper and lower limits of ~45 and ~60 K, respectively. Moreover, the line widths and peak velocities show an overall strong correlation with their rest frequencies, suggesting that the warmer gas is also associated with stronger turbulence effects. The $K = 0$ transitions present a slightly different kinematic signature than the remaining lines, indicating that they might be tracing a different gas component. We speculate that this component is characterized by lower temperatures and therefore larger sizes. Moreover, we predict and discuss the temporal evolution of the CH_3CCH abundance using a two-stage zero-dimensional model of the source constructed with the three-phase Nautilus gas-grain code.

Unified Astronomy Thesaurus concepts: Astrochemistry (75); Collapsing clouds (267); Giant molecular clouds (653); Radio astronomy (1338)

1. Introduction

Star-forming regions play a key role in building the complex inventory of chemical species detected in astronomical environments, which in turn serve as powerful tools to study their surroundings. Through the observation of molecular emission lines, it is possible to constrain both the physical conditions and the chemical evolution of circumstellar sources, shedding light on the formation processes that connect different evolutionary stages of star formation. Methyl acetylene (CH_3CCH), also known as propyne, is a particularly good temperature probe and has therefore been widely explored toward various star-forming objects (e.g., Fontani et al. 2002; Bisschop et al. 2007; Fayolle et al. 2015; Giannetti et al. 2017; Andron et al. 2018; Calcutt et al. 2019).

Massive stars ($L > 10^3$ $L_\odot$; $M > 8$ $M_\odot$) greatly affect their surroundings through their feedback and the production of heavy elements. The formation process of those stars, however, is still less well understood in comparison to the low-mass counterparts. Observational disadvantages, such as their complex cluster environments ($n_* \gtrsim 100$ pc^{-3}) and large distances involved ($d \geqslant 1$ kpc), together with a considerably shorter evolutionary timescale ($t_{KH} \leqslant 10^4$ yr for O-type stars), substantially impair the development of a solid massive-star formation paradigm (Garay & Lizano 1999; Zinnecker & Yorke 2007; Tan et al. 2014; Krumholz 2015, pp 43–80; Silva et al. 2017; Rosen et al. 2020).

Despite the lack of a thoroughly defined evolutionary sequence, some precursors of high-mass stars are well established. One example are hot molecular cores (HMCs), which are one of the first manifestations of massive-star formation (Cesaroni 2005). They are characterized by relatively high temperatures (>100 K) and high densities ($n_{H_2} \sim 10^5$–10^8 cm^{-3}), linked with a compact (<0.1 pc), luminous ($>10^4$ $L_\odot$), and massive (~10–1000 $M_\odot$) molecular core (Heaton et al. 1989; Gomez et al. 1995; Cesaroni et al. 1998; Cesaroni 2005; Bonfand et al. 2019). HMCs are associated with a rich molecular emission spectrum, which carries information on their chemical and physical properties, as well as their morphology and evolutionary stage (e.g., Caselli et al. 1993; Comito et al. 2005; Herbst & van Dishoeck 2009; Allen et al. 2018; Bonfand et al. 2019; Jørgensen et al. 2020; Gieser et al. 2021).

1.1. The Source: G331.512-0.103

G331.512-0.103 (henceforth G331) is a massive and energetic HMC/outflow system. It is located within the millimeter source G331.5-0.1 (see Merello et al. 2013b and references therein), at the tangent point of the Norma spiral arm (~7.5 kpc; Bronfman et al. 1985, 2008), and which consists of a singularly extended and luminous complex at the center of a giant molecular cloud (GMC). The parent GMC is located at the peak region of the southern molecular and massive-star

Original content from this work may be used under the terms of the Creative Commons Attribution 4.0 licence. Any further distribution of this work must maintain attribution to the author(s) and the title of the work, journal citation and DOI.

CH_3CCH

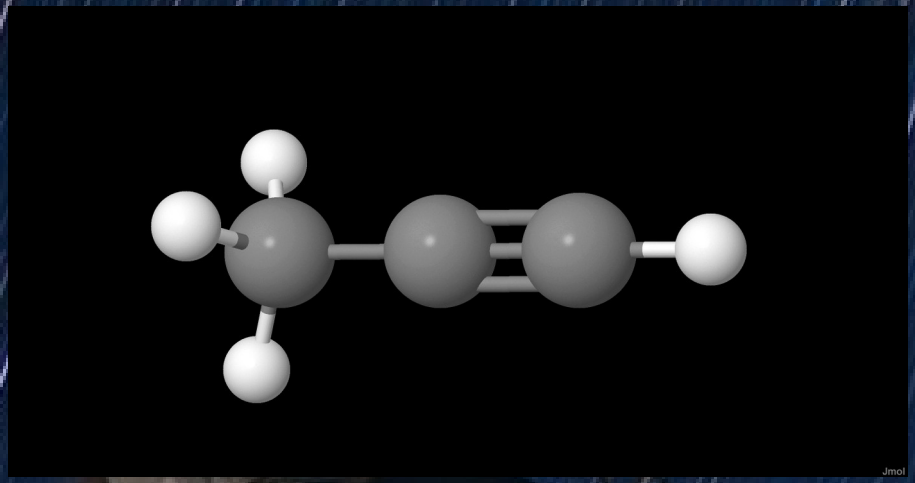

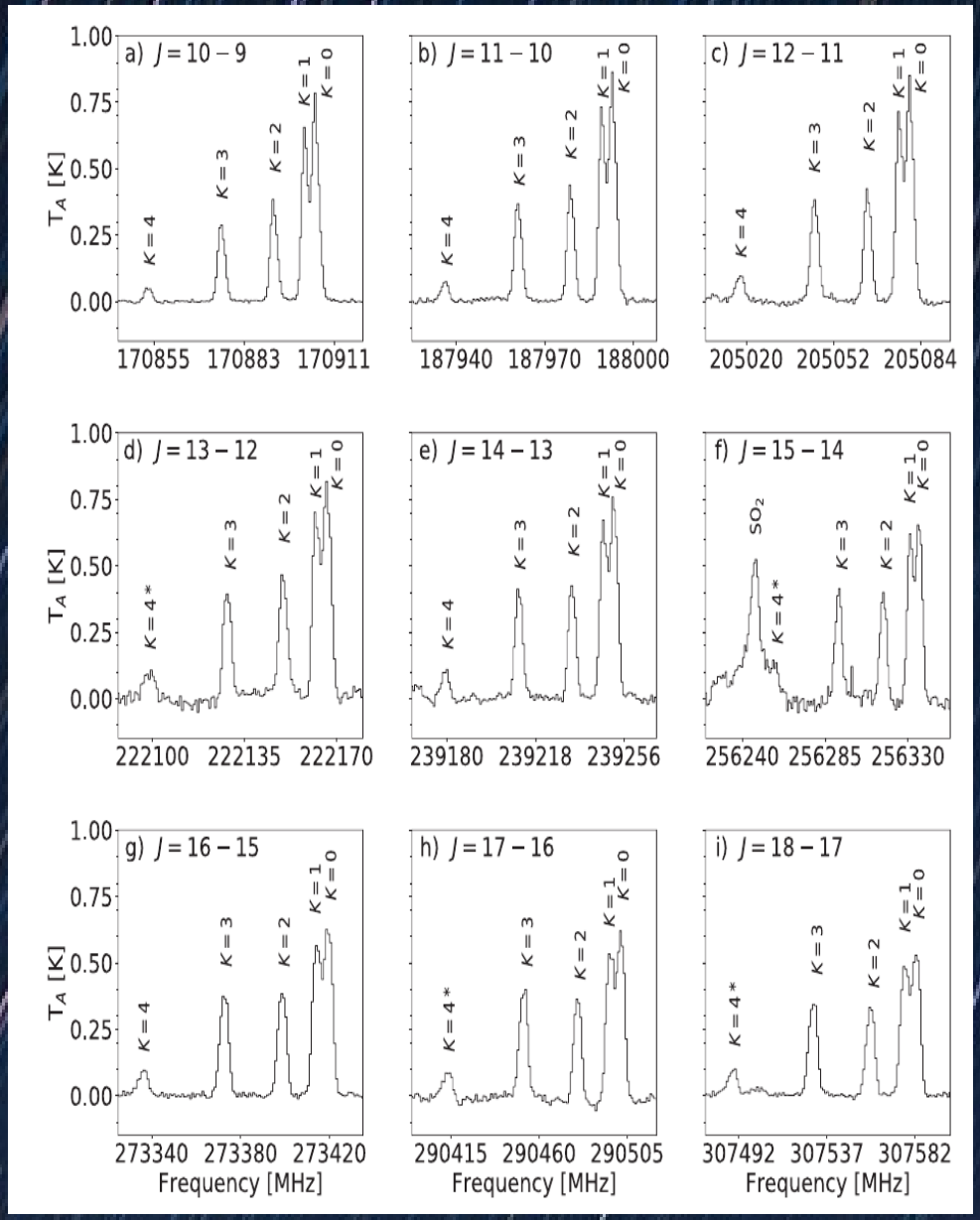

Quantum Numbers				Frequency	E_u	A_u	$\int T_A dv$	V_{lsr}	FWHM
J_u	K_u	J_l	K_l	(MHz)	(K)	(10^{-5} s^{-1})	(K km s^{-1})	(km s^{-1})	(km s^{-1})
10	4	9	4	170,853.576	160.7	1.43	0.24 ± 0.01	−90.02 ± 0.09	4.4 ± 0.2
10	3	9	3	170,876.410	110.1	1.55	1.43 ± 0.01	−89.89 ± 0.02	4.57 ± 0.06
10	2	9	2	170,892.726	74.0	1.63	1.75 ± 0.02	−89.77 ± 0.03	4.41 ± 0.06
10	1	9	1	170,902.518	52.3	1.68	3.04 ± 0.06	−89.74 ± 0.04	4.4 ± 0.1
10	0	9	0	170,905.783	45.1	1.70	3.95 ± 0.04	−89.34 ± 0.02	4.99 ± 0.06
11	4	10	4	187,936.230	169.7	1.97	0.38 ± 0.01	−90.40 ± 0.08	4.76 ± 0.2
11	3	10	3	187,961.342	119.2	2.10	1.87 ± 0.02	−89.96 ± 0.02	4.68 ± 0.05
11	2	10	2	187,979.286	83.0	2.20	2.07 ± 0.02	−89.84 ± 0.02	4.45 ± 0.06
11	1	10	1	187,990.055	61.4	2.25	3.53 ± 0.07	−89.83 ± 0.04	4.6 ± 0.1
11	0	10	0	187,993.645	54.1	2.27	4.43 ± 0.04	−89.39 ± 0.02	5.06 ± 0.06
12	4	11	4	205,018.114	179.6	2.63	0.48 ± 0.01	−89.89 ± 0.07	5.0 ± 0.2
12	3	11	3	205,045.501	129.0	2.77	1.97 ± 0.02	−89.99 ± 0.02	4.80 ± 0.06
12	2	11	2	205,065.070	92.9	2.88	2.04 ± 0.02	−89.86 ± 0.02	4.52 ± 0.05
12	1	11	1	205,076.816	71.2	2.94	3.51 ± 0.06	−89.94 ± 0.04	4.6 ± 0.1
12	0	11	0	205,080.732	64.0	2.96	4.46 ± 0.05	−89.43 ± 0.03	5.18 ± 0.07
13	4	12	4	222,099.153[a]	190.2	3.42	0.72 ± 0.04	−89.9 ± 0.2	6.6 ± 0.4
13	3	12	3	222,128.815	139.7	3.57	1.97 ± 0.04	−90.04 ± 0.04	4.5 ± 0.1
13	2	12	2	222,150.010	103.5	3.69	2.33 ± 0.03	−90.07 ± 0.03	4.84 ± 0.08
13	1	12	1	222,162.730	81.9	3.75	3.74 ± 0.09	−90.15 ± 0.06	5.0 ± 0.1
13	0	12	0	222,166.971	74.6	3.78	4.43 ± 0.06	−89.52 ± 0.03	5.24 ± 0.09
14	4	13	4	239,179.281	201.7	4.34	0.44 ± 0.02	−90.62 ± 0.07	4.1 ± 0.2
14	3	13	3	239,211.215	151.1	4.51	2.02 ± 0.03	−90.15 ± 0.03	4.55 ± 0.07
14	2	13	2	239,234.034	115.0	4.63	2.08 ± 0.03	−90.09 ± 0.03	4.51 ± 0.06
14	1	13	1	239,247.728	93.3	4.70	3.69 ± 0.07	−90.29 ± 0.05	5.2 ± 0.1
14	0	13	0	239,252.294	86.1	4.73	4.25 ± 0.06	−89.50 ± 0.03	5.34 ± 0.09
15	4	14	4	256,258.426[a]	214.0	5.41	1.2 ± 0.1	−89.1 ± 0.3	7.3 ± 0.7
15	3	14	3	256,292.630	163.4	5.59	2.29 ± 0.06	−90.14 ± 0.06	5.1 ± 0.1
15	2	14	2	256,317.071	127.3	5.72	2.13 ± 0.06	−90.02 ± 0.06	4.9 ± 0.1
15	1	14	1	256,331.739	105.7	5.80	3.23 ± 0.06	−90.14 ± 0.04	4.8 ± 0.1
15	0	14	0	256,336.629	98.4	5.83	4.00 ± 0.05	−89.54 ± 0.04	5.43 ± 0.09
16	4	15	4	273,336.519	227.1	6.64	0.58 ± 0.02	−90.30 ± 0.08	5.4 ± 0.2
16	3	15	3	273,372.990	176.6	6.84	2.08 ± 0.02	−90.17 ± 0.03	4.91 ± 0.07
16	2	15	2	273,399.051	140.4	6.97	2.13 ± 0.02	−90.16 ± 0.03	4.93 ± 0.07
16	1	15	1	273,414.692	118.8	7.06	3.48 ± 0.06	−90.42 ± 0.04	5.5 ± 0.1
16	0	15	0	273,419.906	111.5	7.09	3.82 ± 0.02	−89.66 ± 0.02	5.48 ± 0.09
17	4	16	4	290,413.488[a]	241.0	8.04	0.58 ± 0.02	−90.2 ± 0.1	5.3 ± 0.2
17	3	16	3	290,452.224	190.5	8.25	2.40 ± 0.05	−90.47 ± 0.04	5.4 ± 0.1
17	2	16	2	290,479.904	154.4	8.40	2.07 ± 0.03	−90.27 ± 0.03	4.9 ± 0.1
17	1	16	1	290,496.516	132.7	8.49	3.53 ± 0.06	−90.68 ± 0.04	5.7 ± 0.1
17	0	16	0	290,502.054	125.5	8.52	3.81 ± 0.05	−89.88 ± 0.04	5.4 ± 0.1
18	4	17	4	307,489.264[a]	255.8	9.62	0.52 ± 0.01	−90.13 ± 0.07	5.2 ± 0.2
18	3	17	3	307,530.263	205.3	9.84	1.88 ± 0.02	−90.23 ± 0.03	4.90 ± 0.06
18	2	17	2	307,559.559	169.1	10.00	1.73 ± 0.02	−90.23 ± 0.03	4.76 ± 0.07
18	1	17	1	307,577.141	147.5	10.10	2.91 ± 0.04	−90.50 ± 0.03	5.39 ± 0.08
18	0	17	0	307,583.003	140.3	10.10	3.27 ± 0.05	−89.76 ± 0.04	5.6 ± 0.1

LTE

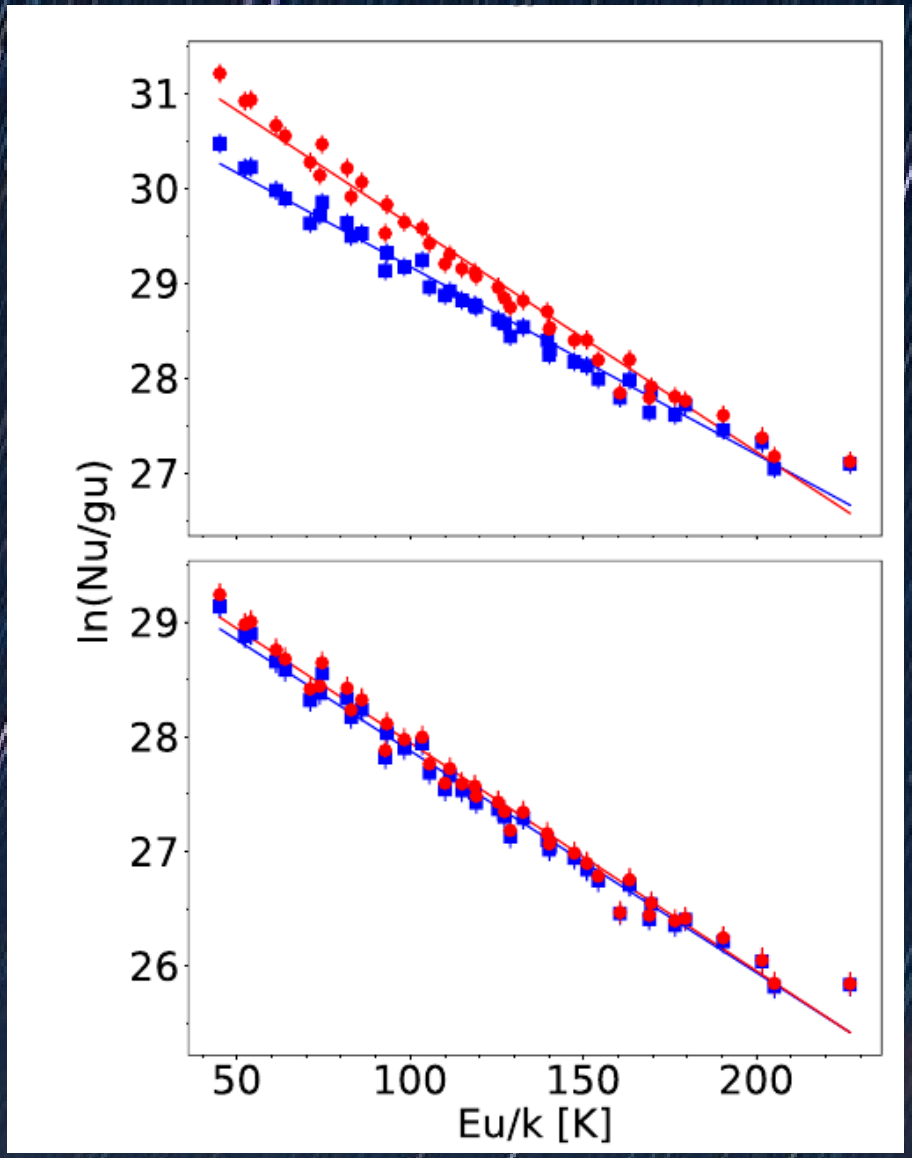

Parameter	Source Size: 5″		Source Size: 10″	
	With C_τ	Without C_τ	With C_τ	Without C_τ
T_{exc} (K)	42 ± 1	51 ± 1	50 ± 1	52 ± 1
N ($\times 10^{16}$ cm^{-2})	4.5 ± 0.3	2.5 ± 0.1	0.75 ± 0.04	0.69 ± 0.04
χ^2_{red}	2.57	1.49	1.51	1.42

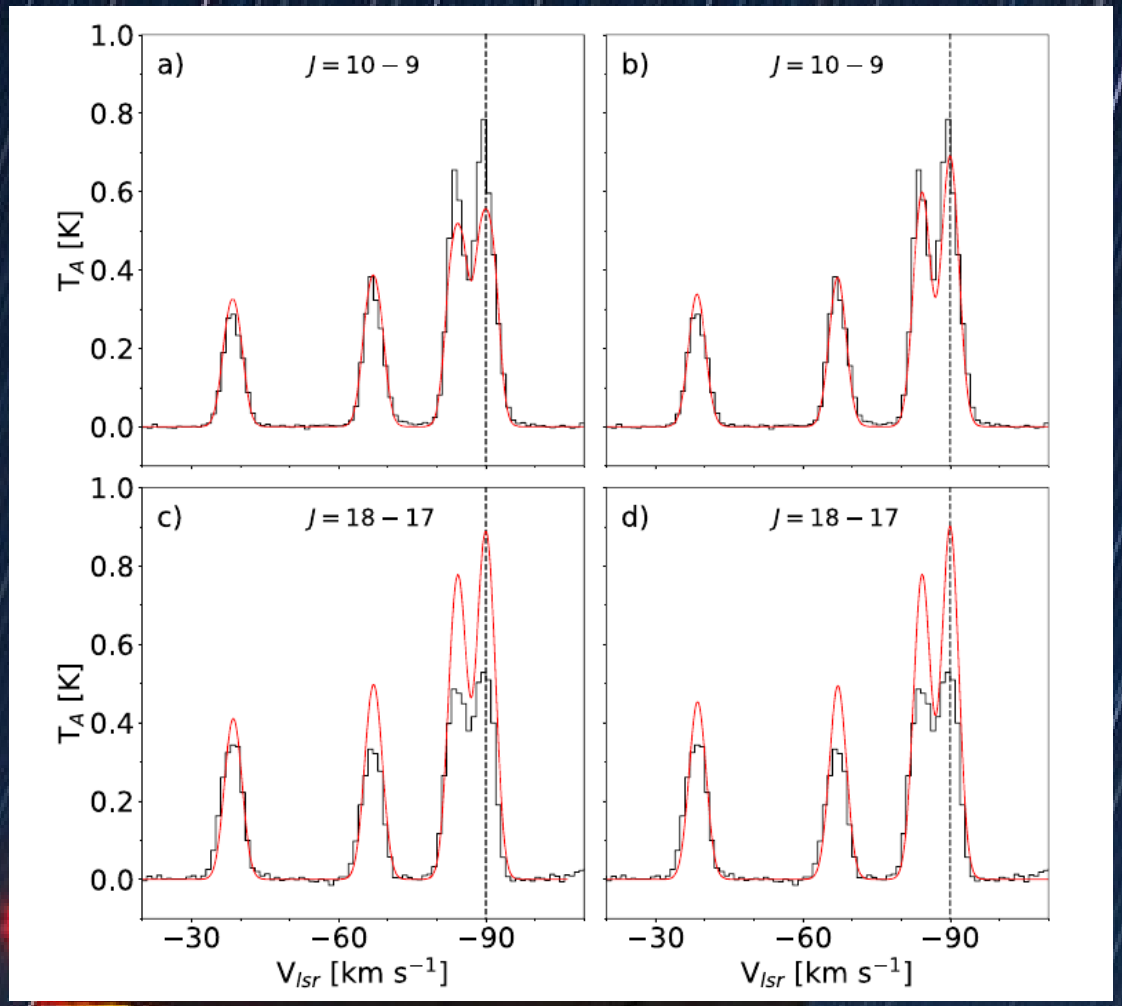

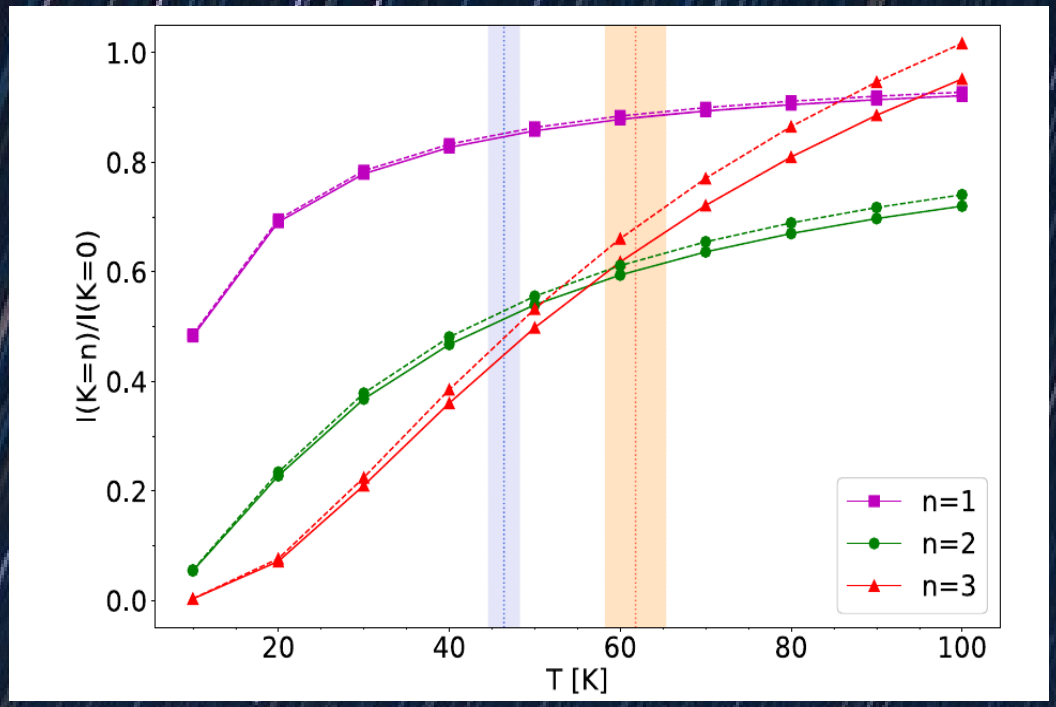

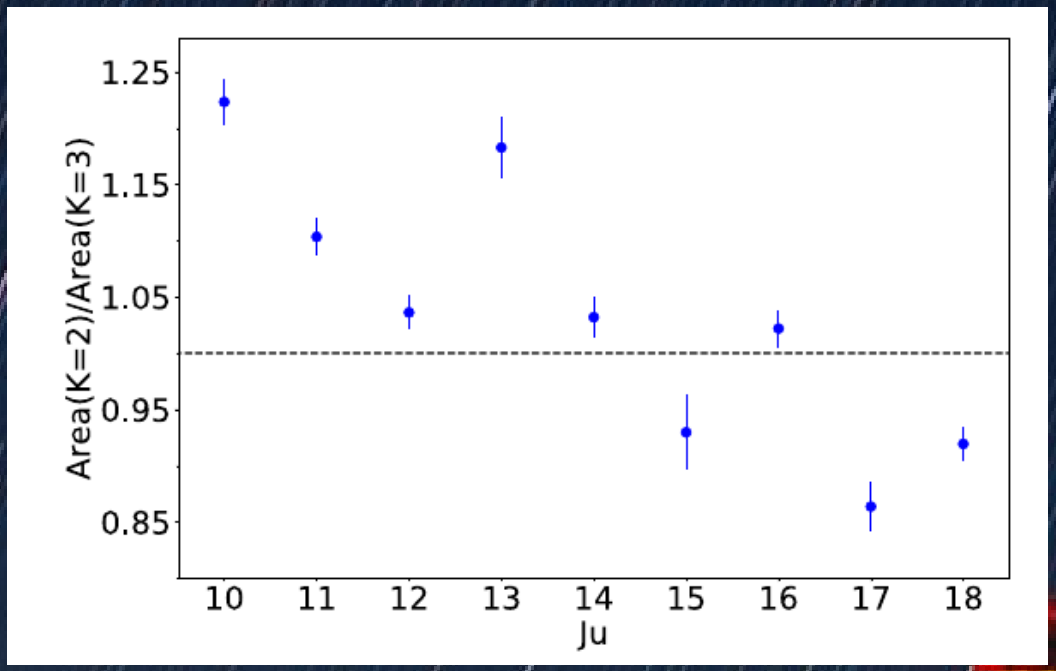

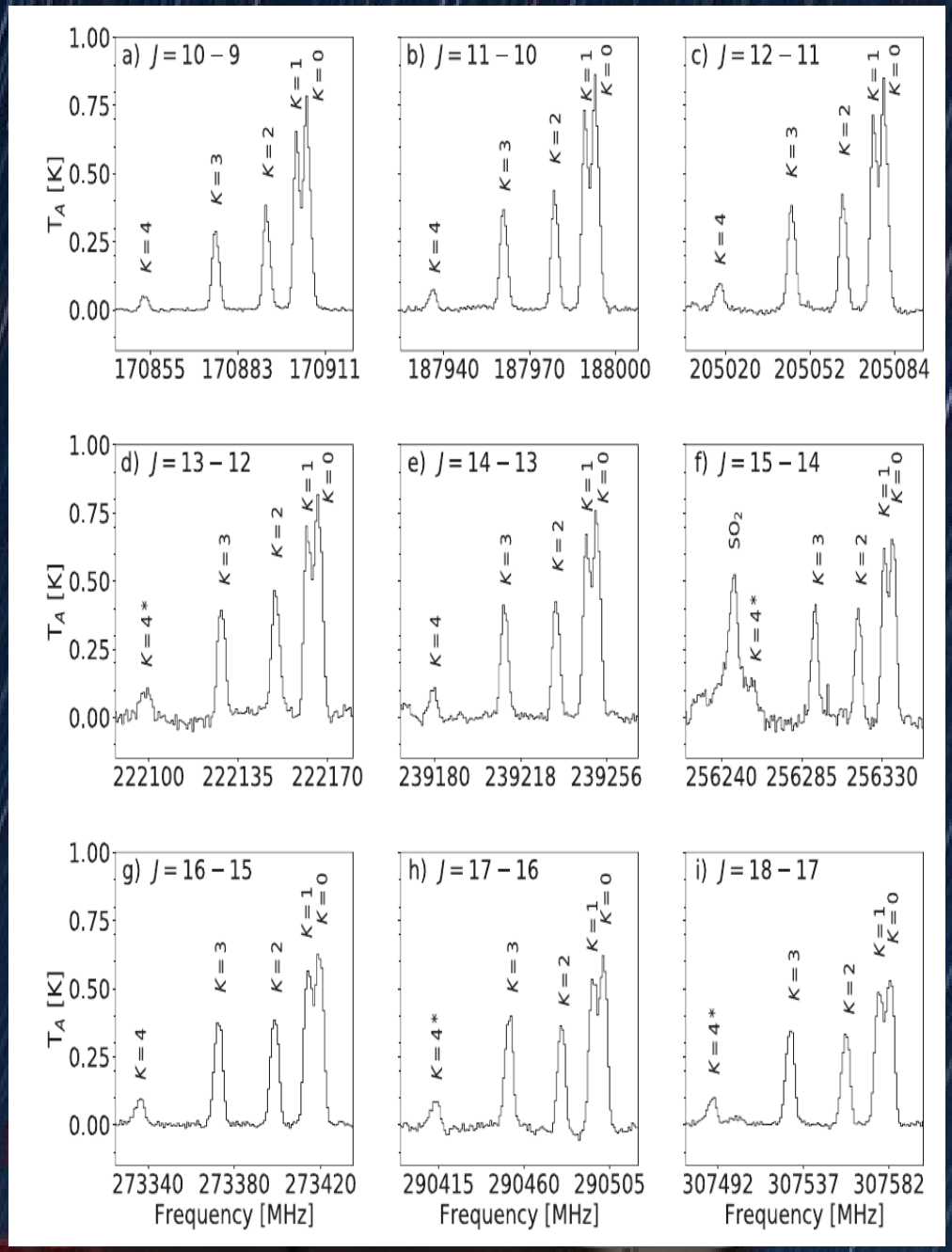

Science with LLAMA. September 5-9 2022. Salta, Argentina

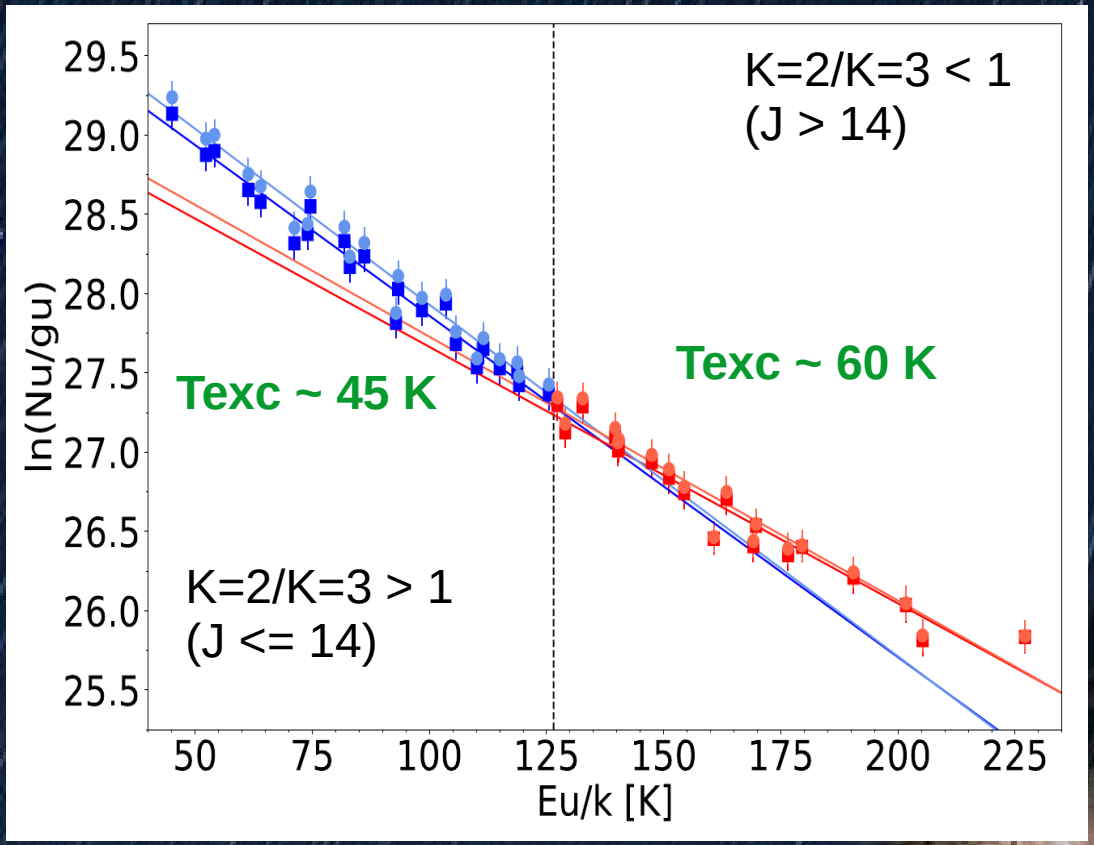
K=2/K=3 < 1
(J > 14)
Texc ~ 60 K
Texc ~ 45 K
K=2/K=3 > 1
(J <= 14)
ln(Nu/gu)
Eu/k [K]
29.5
29.0
28.5
28.0
27.5
27.0
26.5
26.0
25.5
50
75
100
125
150
175
200
225

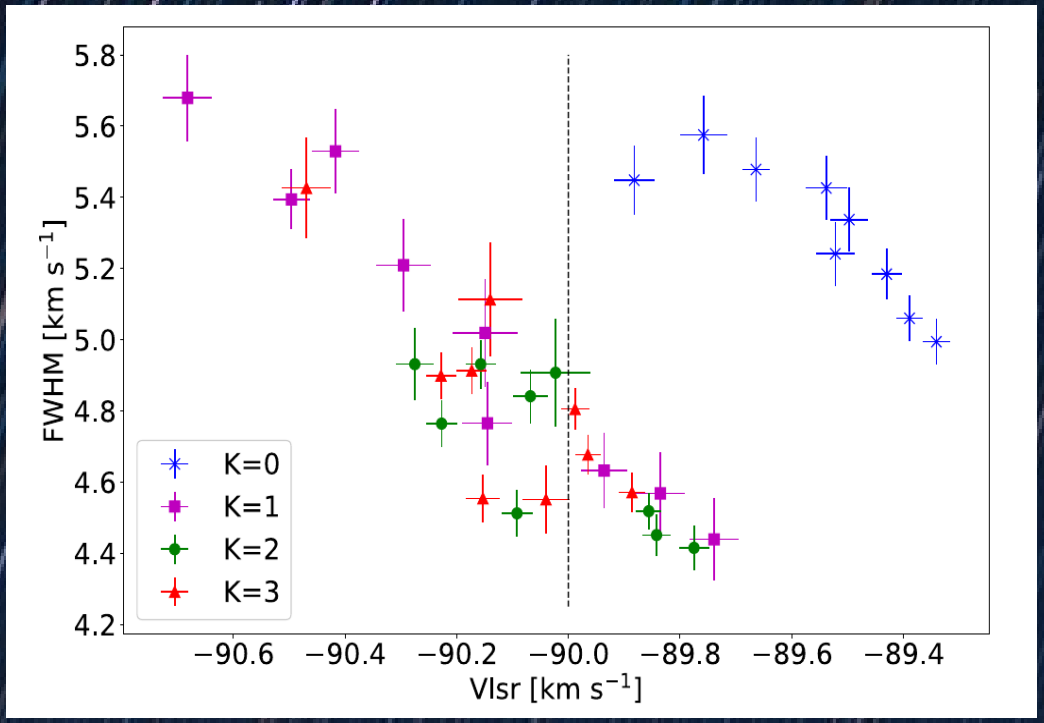

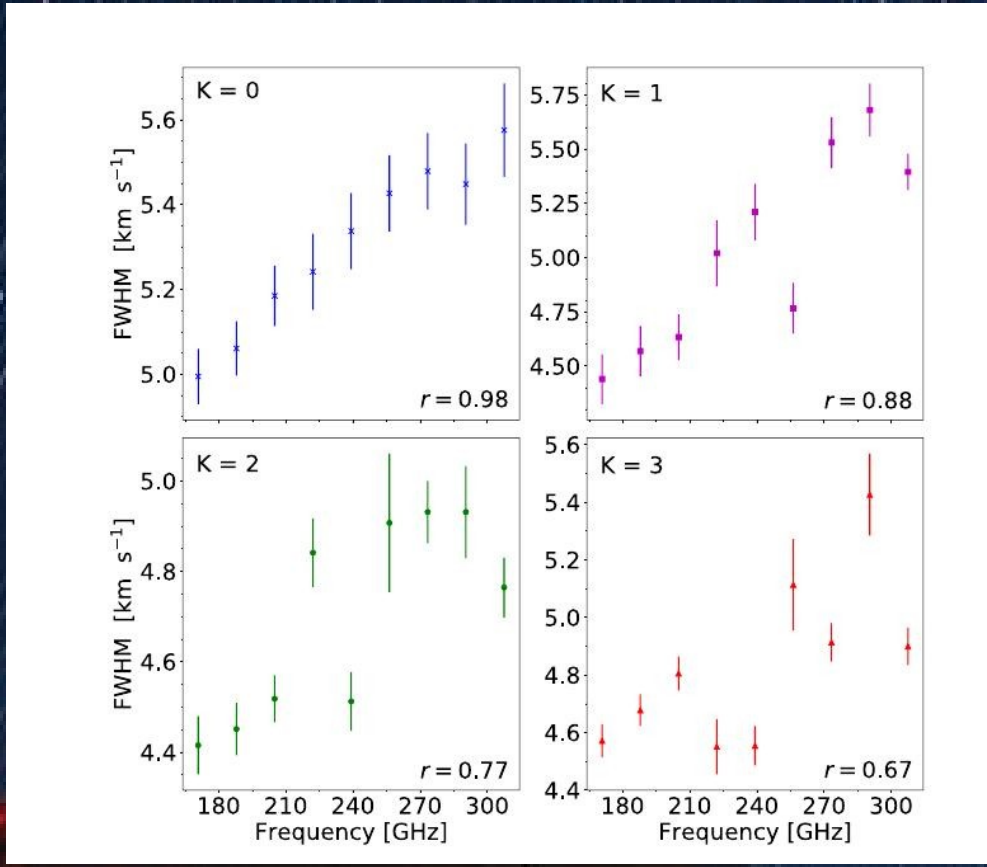

Science with LLAMA. September 5-9 2022. Salta, Argentina

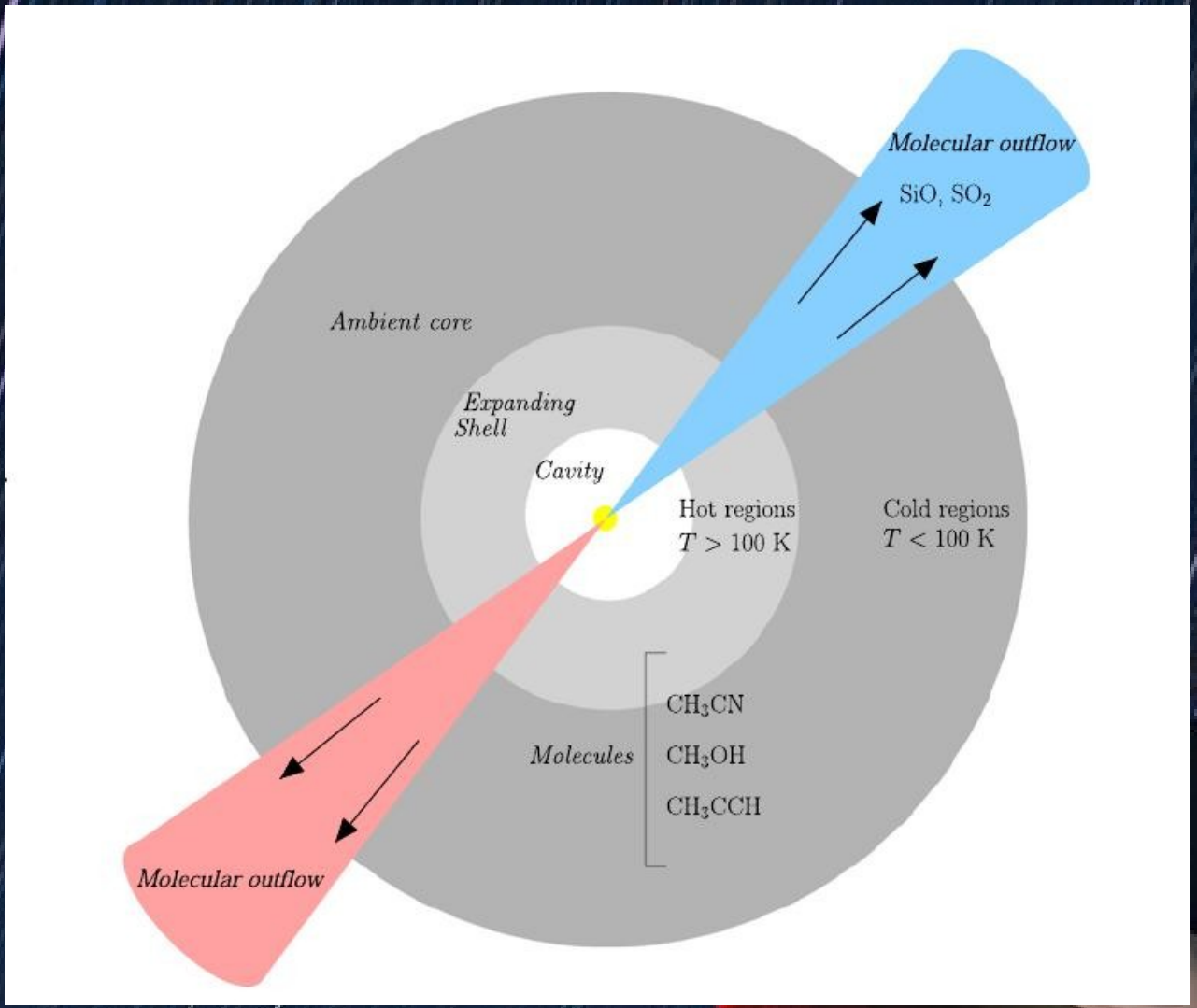
Molecular outflow
SiO, SO_2
Ambient core
Expanding Shell
Cavity
Hot regions
$T > 100$ K
Cold regions
$T < 100$ K
CH_3CN
Molecules
CH_3OH
CH_3CCH
Molecular outflow

Thank you!

Science with LLAMA. September 5-9 2022. Salta, Argentina